Detailed investigation of low-energy positronium-hydrogen scattering

Denton Woods, S. J. Ward, and P. Van Reeth

Phys. Rev. A **92**, 022713 — Published 28 August 2015

DOI: 10.1103/PhysRevA.92.022713

Detailed Investigation of Low-Energy Positronium-Hydrogen Scattering

Denton Woods* and S. J. Ward†

Department of Physics, University of North Texas, Denton, Texas 76203, USA

P. Van Reeth

Department of Physics and Astronomy, University College London, Gower Street, London WC1E 6BT, UK

(Dated: July 29, 2015)

Abstract

We investigate the four-body Coulomb process of low-energy elastic positronium-hydrogen (Ps-H) scattering below the Ps(n=2) excitation threshold using scattering wavefunctions that include Hylleraas-type correlation terms. Using the complex Kohn variational method, we compute phase shifts through the $^{1,3}H$-wave and obtain highly accurate $^{1,3}S$- and $^{1,3}P$-wave phase shifts. The complex Kohn variational results compare well to a number of other calculations for this system. We present elastic differential, elastic integrated, and momentum transfer cross sections, and for the singlet, resonances through the ^{1}F-wave. The differential cross section exhibits interesting features, including a change from slightly backward peaked to forward peaked scattering as the energy of the incident positronium increases and rich structure due to multiple resonances near the Ps(n=2) threshold. We also give a detailed analysis of the scattering lengths and effective ranges using multiple effective range theories.

PACS numbers: 31.15.xt Variational techniques; 34.50.-s Scattering of atoms and molecules; 36.10.Dr Positronium; 34.80.Bm Elastic scattering

Keywords: positronium; PsH; positronium hydride; Kohn variational

* denton.woods@unt.edu; http://www.dentonwoods.com

† Corresponding author: sward@unt.edu

I. INTRODUCTION

Positronium (Ps) scattering from atoms and molecules is an area of current experimental and theoretical interest. The development of energy-tunable ortho-Ps beams [1–5] has enabled measurements to be made of Ps scattering from the inert gases He, Ne, Ar, Kr, and Xe [4–11] and the molecules H_2, N_2, O_2, CO_2, H_2O, and SF_6 [4, 6, 8, 9, 11–13]. Cross sections for Ps scattering from H have not been measured due to the difficulty of creating an atomic H beam, although the binding energy of positronium hydride (PsH) has been measured in the reaction of a positron with methane, $e^+ + CH_4 \rightarrow CH_3^+ + PsH$ [14]. The low-energy region is of particular interest, because in this energy range, positron and electron correlations are important. We present our work of the application of the S-matrix complex Kohn variational method to elastic Ps(1s)-H(1s) scattering for the energy range up to the excitation threshold of Ps(n=2) at $\frac{3}{16}$ a.u. (5.102 eV) [15–20].

Ps-H scattering is a fundamental four-body Coulomb process. The Kohn and inverse Kohn variational methods have previously been applied to Ps-H collisions by Van Reeth and Humberston [21, 22], who computed $^{1,3}S$ and $^{1,3}P$ phase shifts. We extend their $^{1,3}S$ and $^{1,3}P$ variational calculations in multiple ways. In addition to the Kohn and inverse Kohn variational methods, we implement the generalized Kohn method, and the complex Kohn methods for the S and T matrices. The complex Kohn methods for the S and T matrices are known to suffer from far fewer anomalous singularities than the Kohn, inverse Kohn and generalized Kohn variational methods [23–25]. Another extension that we consider is to use the procedure by Todd [26] to systematically remove short-range terms that cause linear dependence. This enables us to compute the phase shifts with more short-range Hylleraas terms than the earlier Kohn and inverse Kohn variational calculations [21, 22]. We add the asymptotic expansion of Drake and Yan [27, 28] to improve the accuracy of matrix elements containing only short-range terms. We significantly increase the number of integration points for matrix elements that involve the long-range terms, along with implementing a procedure to accelerate the convergence of these integrals (introduction and subsequent removal of exponential terms to the Gauss-Laguerre quadratures). We also extend the calculations to the next four partial waves through to the H-wave, which enables us to calculate the elastic differential, elastic integrated, and momentum transfer cross sections.

We present in this paper results we generally obtain using the S-matrix complex Kohn

variational method for Ps-H scattering. We confirm the previously calculated resonances for the first four partial waves and compare the resonance parameters to those of the earlier Kohn [22], close coupling (CC) [29] and complex rotation calculations [30–33]. In addition, we compute the scattering lengths and effective ranges using multiple effective range theories.

We use the short-range part of the full scattering wavefunction to compute the binding energy of PsH. The binding energy of PsH, E_b, has been calculated using various methods. Ho [34] performed a variational calculation with a Hylleraas-type basis set, and Yan and Ho [30] later did a more extensive calculation. Mitroy [35] used the stochastic variational method (SVM) with 1800 explicitly correlated Gaussians (ECGs), and Bubin and Adamowicz [36] found the most accurate value to date using 5000 ECGs in a variational calculation.

There have been a number of other calculations for Ps-H scattering. A much earlier Kohn variational calculation was performed by Page [37] for the Ps-H scattering lengths. Drachman and Houston [38, 39] used a stabilization method with an effective range theory (ERT) expansion. At low energies, diffusion Monte Carlo (DMC) [40], the SVM [41, 42], CC [29, 43–48], static exchange [49, 50], Kohn variational [21, 22, 37], and inverse Kohn variational [21, 22] methods have been applied. The SVM with stabilization techniques was used to compute low-energy phase shifts and scattering lengths for Ps-H collisions [41, 42].

Massey and Mohr [51] considered Ps-H inelastic scattering using the first Born approximation and computed the elastic cross section by making use of the Born-Oppenheimer (BO) approximation [51–56]. More recently, McAlinden et al. [57] applied the first Born approximation to compute the total cross section for Ps(1s)-H(1s) scattering. Blackwood et al. [47] performed an elaborate CC calculation for Ps scattering from H, which took into account excitation and ionization of both the projectile and target. They considered two different coupling schemes. The first one, which they refer to as 9Ps9H, included 9 eigen- and pseudo-states of Ps and also of H. The second scheme, which they refer to as 14Ps14H, was used for S-wave scattering only and included 14 eigen- and pseudo-states of Ps and also of H. Good agreement was obtained between the CC [47] and the SVM [42] for the $^{1,3}S$-wave scattering lengths and phase shifts. In another paper, Blackwood et al. [48] considered the importance of including the H^- channel in a 22Ps1H coupling scheme, comparing with the previous 22Ps1H calculations of Campbell et al. [44]. Walters et al. [29] extended the earlier CC calculations [47] to include the e^+-H^- channel [48] and compared their results for the S-wave with the Kohn variational results [21]. A recent calculation of Ps-H scattering by

Zhang and Yan [58] used the confined variational method (CVM) to calculate phase shifts for two momenta for both ^1S and ^3S. This method provides accurate results but has the drawback of being very computationally expensive.

The Kohn variational method gives rigorous upper bounds on the scattering lengths and, except for Schwartz singularities, empirical lower bounds on the phase shifts. This means that the wavefunction can be systematically improved to the converged results. The Kohn and inverse Kohn variational methods are known to yield accurate results and have provided benchmark results [21, 22] with which results from other calculations can be compared.

We express phase shifts in radians and use atomic units throughout unless we state otherwise. For conversions to electron-volts (eV), we use the conversion factor 1 a.u. = 27.21138505(60) eV [59].

II. THEORY

A. The Positronium-Hydrogen System and Trial Scattering Wavefunctions

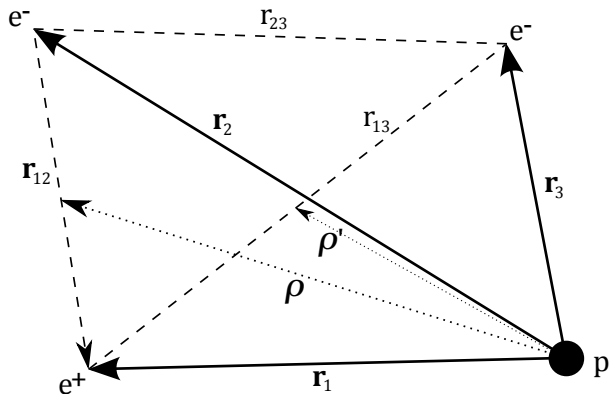

FIG. 1: Positronium-hydrogen coordinate system

We investigate low-energy elastic scattering of ground-state Ps with ground-state H, Ps(1s)+H(1s), for incident energies up to the excitation threshold of Ps(n=2). Previous work on Ps-H scattering used the Kohn and inverse Kohn variational methods [21, 22]. Van Reeth and Humberston [60] used the complex Kohn variational method for e^+-He scattering. While we generally present results in Sec. IV that we obtain using the S-matrix complex Kohn variational method, in this section we present a general wavefunction that can be used

in the Kohn variational method and a number of its variants, as we describe in Sec. II B.

For S-wave Ps(1s)-H(1s) elastic scattering, the flexible scattering wavefunction is given by

$$\Psi_0^{\pm,t} = \widetilde{S}_0 + L_0^{\pm,t}\,\widetilde{C}_0 + \sum_{i=1}^{N(\omega)} c_{i0}^{\pm}\bar{\phi}_{i01}, \tag{1}$$

where the superscript t indicates that this is a trial wavefunction. The plus sign indicates the spatially symmetric singlet case, and the minus sign indicates the spatially antisymmetric triplet case. The total orbital angular momentum of the system is equal to the orbital angular momentum ℓ of the incoming Ps(1s). We choose for the z-component of the total orbital angular momentum to be zero because of axial symmetry of the scattering system [61]. For a trial wavefunction of total orbital momentum equal to ℓ, there are $\ell+1$ types of short-range terms of different symmetries [62–68]. However, for partial waves $\ell > 0$, we consider a trial wavefunction of the form

$$\Psi_\ell^{\pm,t} = \widetilde{S}_\ell + L_\ell^{\pm,t}\,\widetilde{C}_\ell + \sum_{i=1}^{N(\omega)} c_{i\ell}^{\pm}\bar{\phi}_{i\ell1} + \sum_{i=N(\omega)+1}^{2N(\omega)} d_{i\ell}^{\pm}\bar{\phi}_{i\ell2}, \tag{2}$$

where we neglect mixed symmetry terms for $\ell \geq 2$ as we discuss later in this section. The scattering wavefunctions contain both the long-range terms $\widetilde{S}_\ell$ and $\widetilde{C}_\ell$ and the short-range terms $\bar{\phi}_{i\ell k}$. The long-range terms of Eqs. (1) and (2) are given by

$$\begin{bmatrix} \widetilde{S}_\ell \\ \widetilde{C}_\ell \end{bmatrix} = \mathbf{u} \begin{bmatrix} \bar{S}_\ell \\ \bar{C}_\ell \end{bmatrix} = \begin{bmatrix} u_{00} & u_{01} \\ u_{10} & u_{11} \end{bmatrix} \begin{bmatrix} \bar{S}_\ell \\ \bar{C}_\ell \end{bmatrix}, \tag{3}$$

where

$$\bar{S}_\ell = \frac{1 \pm P_{23}}{\sqrt{2}} Y_{\ell0}(\theta_\rho, \varphi_\rho)\Phi_{\mathrm{Ps}(1s)}(r_{12})\,\Phi_{\mathrm{H}(1s)}(r_3)\,\sqrt{2\kappa}\,j_\ell\,(\kappa\rho) \tag{4}$$

and

$$\bar{C}_\ell = -\frac{1 \pm P_{23}}{\sqrt{2}} Y_{\ell0}(\theta_\rho, \varphi_\rho)\Phi_{\mathrm{Ps}(1s)}(r_{12})\,\Phi_{\mathrm{H}(1s)}(r_3)\,\sqrt{2\kappa}\,n_\ell\,(\kappa\rho)\,f_\ell(\rho). \tag{5}$$

Fig. 1 gives the coordinate system for Ps-H. The vector $\boldsymbol{\rho} = \frac{1}{2}\,(\boldsymbol{r_1} + \boldsymbol{r_2})$ is the position vector of the center of mass of the Ps atom with respect to the proton, $j_\ell\,(\kappa\rho)$ and $n_\ell\,(\kappa\rho)$ are the spherical Bessel and Neumann functions respectively, and $Y_{\ell m}(\theta_\rho, \varphi_\rho)$ is the spherical harmonic, for which we use $m = 0$. P_{23} is the exchange operator for the two indistinguishable electrons, $\boldsymbol{\kappa}$ is the momentum of the incoming Ps(1s) atom, and $\Phi_{\mathrm{Ps}(1s)}(r_{12})$ and $\Phi_{\mathrm{H}(1s)}(r_3)$ are the ground-state wavefunctions of Ps and H, respectively. The shielding factor, $f_\ell(\rho)$,

removes the singularity of the spherical Neumann function at the origin. We choose it to have the form

$$f_\ell(\rho) = \left[1 - \, \mathrm{e}^{-\mu\rho}\left(1 + \frac{\mu}{2}\rho\right)\right]^{m_\ell}. \tag{6}$$

Table I shows the values of the nonlinear parameter μ and the integer power m_ℓ that we use for each partial wave. The value of m_ℓ is greater than or equal to $(2\ell+1)$, and if $m_\ell = (2\ell+1)$, then the leading term of $n_\ell(\kappa\rho)\, f_\ell(\rho)$ corresponds to the leading term of $j_\ell(\kappa\rho)$ as $\rho \to 0$.

We consider the Kohn variational method and a number of its variants, and $\mathbf{u}$ and $L_\ell^\pm$ take different forms depending on which one:

$$\text{generalized Kohn, } L_\ell^{\pm,t} = \tan(\delta_\ell^{\pm,t} - \tau), \mathbf{u} = \left[\begin{smallmatrix} \cos\tau & \sin\tau \\ -\sin\tau & \cos\tau \end{smallmatrix}\right], \tag{7a}$$

$$\text{generalized } T\text{-matrix complex Kohn, } L_\ell^{\pm,t} = T_\ell^\pm, \mathbf{u} = \left[\begin{smallmatrix} \cos\tau & \sin\tau \\ -\sin\tau + \mathrm{i}\cos\tau & \cos\tau + \mathrm{i}\sin\tau \end{smallmatrix}\right] \tag{7b}$$

$$\text{generalized } S\text{-matrix complex Kohn, } L_\ell^{\pm,t} = -S_\ell^\pm, \mathbf{u} = \left[\begin{smallmatrix} -\mathrm{i}\cos\tau - \sin\tau & -\mathrm{i}\sin\tau + \cos\tau \\ \mathrm{i}\cos\tau - \sin\tau & \mathrm{i}\sin\tau + \cos\tau \end{smallmatrix}\right]. \tag{7c}$$

For the case of $\tau = 0$, these give the Kohn, the T-matrix and S-matrix complex Kohn variational methods, respectively. $\tau = \frac{\pi}{2}$ in Eq. (7a) gives the inverse Kohn. For comparison with Cooper et al. [25], the generalized Kohn $\mathbf{u}$ matrix is identical to their corresponding matrix, while the $\mathbf{u}$ matrix for the generalized T-matrix complex Kohn is similar to their corresponding matrix. We use the definition of the T and S matrices given by Bransden [56]. The $\mathbf{u}$ matrix for the Kohn in Eq. (7) is identical to that of Lucchese [23], but the $\mathbf{u}$ matrices for the inverse Kohn, T-matrix complex Kohn, and S-matrix complex Kohn are slightly different.

The short-range terms are highly correlated Hylleraas-type functions, including all interparticle distances, given by

$$\begin{aligned} \bar{\phi}_{i\ell k} = &\left(1 \pm P_{23}\right) Y_{\ell 0}(\theta_k, \phi_k) e^{-(\alpha r_1 + \beta r_2 + \gamma r_3)} \\ &\times r_k^\ell r_1^{k_i} r_2^{l_i} r_{12}^{m_i} r_3^{n_i} r_{13}^{p_i} r_{23}^{q_i}. \end{aligned} \tag{8}$$

The variable ω is a non-negative integer that determines the maximum number of terms in the basis set. For a chosen value of ω, the integer powers of r_i and r_{ij} are constructed in such a way that

$$k_i + l_i + m_i + n_i + p_i + q_i \leq \omega, \tag{9}$$

with all k_i, l_i, m_i, n_i, q_i and $p_i \geq 0$ [22]. The first set of short-range terms in Eq. (2), which we refer to as the first symmetry, has $k = 1$ for $i = 1$ to $N(\omega)$. The second symmetry set

of terms exists for $\ell > 0$, with $k = 2$ and $i = N(\omega) + 1$ to $2N(\omega)$. These short-range terms represent the orbital angular momentum as being placed mainly on either the positron ($\boldsymbol{r}_1$) or on the electron in the Ps atom ($\boldsymbol{r}_2$, and $\boldsymbol{r}_3$ with exchange). Van Reeth and Humberston [22] discussed the slow convergence of their ^3P phase shifts and suggested having a trial wavefunction in which the orbital angular momentum is placed mainly on the electron of the H atom ($\boldsymbol{r}_3$, and $\boldsymbol{r}_2$ with exchange) and on the Ps atom ($\boldsymbol{\rho}$, and $\boldsymbol{\rho}'$ with exchange). We implement their suggestion for the singlet and triplet P-waves [20]. For $\omega = 6$, we find that the phase shifts we obtain with the alternative form of the trial wavefunction are comparable to the phase shifts we obtain, and present in this paper, using the trial wavefunction Eq. (2) with $\ell = 1$ [20]. In Sec. III, we discuss numerical techniques that enable us to achieve well converged $^{1,3}P$-wave phase shifts.

For the D-wave and higher partial waves, we do not include short-range terms of mixed symmetry [62]. These, however, have been included for the three-body system of e^+-H for the D-wave in earlier work given in Refs. [63–67]. Van Reeth and Humberston [67] found that these mixed symmetry terms contributed less than 1.5% to the K-matrix elements for e^+-H scattering, but this result now appears to be in error. A preliminary investigation for e^+-H [69] with a corrected code has shown that these mixed symmetry terms can be important for that system. This investigation found that including the mixed symmetry terms changes the phase shifts by less than 1% at $\kappa = 0.1$, and near the Ps formation threshold, by about 10%. Fortunately, in the earlier D-wave e^+-H scattering calculation [66], the inclusion of the virtual Ps terms represented sufficiently well the required spatial configuration so that it compensated for the lack of convergence due to the error in the previous inclusion of the mixed symmetry terms. The final numerical results used in Ref. [67] are within 1 to 2% of the phase shifts of the preliminary calculation [69] that correctly includes the mixed symmetry terms and for which the virtual Ps terms have been found to make no significant contribution. The investigation of Ref. [69] has been extended to e^--H scattering, and it has revealed that for the ^1D-wave, the inclusion of the mixed symmetry terms has little effect on the phase shifts at very low energies but has a more appreciable effect at higher energy. Interestingly, the investigation found that the mixed symmetry terms change the ^3D-wave e^--H phase shifts less than 1% over the energy range considered. As discussed in Sec. IV for Ps-H scattering, the D-wave contributes only a small amount to the elastic integrated cross sections away from the ^1D resonance. Therefore, due to the complexity of including the

mixed symmetry terms for the four-body system, we do not explicitly include these terms for Ps-H scattering for the D-wave or for any partial wave $\ell \geq 2$. For $\ell \geq 1$, we use the trial wave function we give in Eq. (2).

The Hamiltonian for the Ps-H system is

$$H = -\frac{1}{2}\nabla^2_{\boldsymbol{r}_1} - \frac{1}{2}\nabla^2_{\boldsymbol{r}_2} - \frac{1}{2}\nabla^2_{\boldsymbol{r}_3} + \frac{1}{r_1} - \frac{1}{r_2} - \frac{1}{r_3} - \frac{1}{r_{12}} - \frac{1}{r_{13}} + \frac{1}{r_{23}}, \tag{10}$$

which, using Jacobi coordinates for the kinetic energy operator, can be expressed as

$$H = -\frac{1}{4}\nabla^2_{\boldsymbol{\rho}} - \frac{1}{2}\nabla^2_{\boldsymbol{r}_3} - \nabla^2_{\boldsymbol{r}_{12}} + \frac{1}{r_1} - \frac{1}{r_2} - \frac{1}{r_3} - \frac{1}{r_{12}} - \frac{1}{r_{13}} + \frac{1}{r_{23}}. \tag{11}$$

B. Derivation of the Kohn Variational Method and Variants of the Method

The derivation we present here for the Kohn variational method and its variants follows a similar procedure given in Refs. [23, 25, 61, 68]. The functional for the full scattering wavefunction in Eqs. (1) and (2) is (dropping the ℓ subscript and the $\pm$ superscript for brevity),

$$I[\Psi^t] = \left(\Psi^t, \mathcal{L}\Psi^t\right) = \int \Psi^t \mathcal{L} \Psi^t \, d\tau, \tag{12}$$

with

$$\mathcal{L} = 2(H - E). \tag{13}$$

The total energy of the system, E, is given by

$$E = E_H + E_{Ps} + \frac{1}{4}\kappa^2 = E_H + E_{Ps} + E_{\boldsymbol{\kappa}}, \tag{14}$$

where E_H and E_{Ps} are the ground-state energies of H and Ps, respectively, and $E_{\boldsymbol{\kappa}}$ is the kinetic energy of the incoming Ps atom. The complex conjugate of Ψ^t that premultiplies $\mathcal{L}\Psi^t$ is not taken for a consistent derivation of the complex Kohn variational methods [23, 25].

We assume the trial wavefunction Ψ^t is a small variation of the exact wavefunction Ψ, or

$$\Psi^t = \Psi + \delta\Psi. \tag{15}$$

It can be shown that the variation in the functional I, $\delta I = I[\Psi^t] - I[\Psi] = I[\Psi^t]$, is given by

$$\delta I = (L^t - L) \det \mathbf{u} + I[\delta\Psi]. \tag{16}$$

Here L^t represents the scattering parameters given by Eq. (7) for the trial wavefunctions given by Eqs. (1) and (2), and L represents the corresponding parameters (given by Eq. (7) without the 't') for the exact wavefunction. Neglecting the second-order term in $\delta\Psi$, $I[\delta\Psi]$, and realizing that $I[\Psi] = 0$, we obtain a functional for the variational L^v of

$$L^v = L^t - I[\Psi^t]/\det \mathbf{u}. \tag{17}$$

Using the stationary property of the functional, we take the derivative of L^v with respect to the linear parameters and set the derivatives to zero, i.e. for the S-wave

$$\frac{\partial L^v}{\partial L^t} = 0 \text{ and } \frac{\partial L^v}{\partial c_i} = 0 \text{ where } i = 1, \ldots, N(\omega). \tag{18}$$

Eq. (18) yields the matrix equation for the S-wave of

$$\begin{bmatrix} (\widetilde{C}, \mathcal{L}\widetilde{C}) & (\widetilde{C}, \mathcal{L}\bar{\phi}_{101}) & \cdots & (\widetilde{C}, \mathcal{L}\bar{\phi}_{N01}) \\ (\bar{\phi}_{101}, \mathcal{L}\widetilde{C}) & (\bar{\phi}_{101}, \mathcal{L}\bar{\phi}_{101}) & \cdots & (\bar{\phi}_{101}, \mathcal{L}\bar{\phi}_{N01}) \\ \vdots & \vdots & \ddots & \vdots \\ (\bar{\phi}_{N01}, \mathcal{L}\widetilde{C}) & (\bar{\phi}_{N01}, \mathcal{L}\bar{\phi}_{101}) & \cdots & (\bar{\phi}_{N01}, \mathcal{L}\bar{\phi}_{N01}) \end{bmatrix} \begin{bmatrix} L^t \\ c_1 \\ \vdots \\ c_N \end{bmatrix} = - \begin{bmatrix} (\widetilde{C}, \mathcal{L}\widetilde{S}) \\ (\bar{\phi}_{101}, \mathcal{L}\widetilde{S}) \\ \vdots \\ (\bar{\phi}_{N01}, \mathcal{L}\widetilde{S}) \end{bmatrix}. \tag{19}$$

This matrix equation can be rewritten as $\boldsymbol{AX} = \text{-}\boldsymbol{B}$, as can the corresponding matrix equations for $\ell > 0$. For higher partial waves, the matrix equation looks the same but includes the second symmetry short-range terms and corresponding coefficients. Finally, for arbitrary ℓ, we solve for L^v,

$$L^v = -\frac{1}{\det \mathbf{u}} \left(\boldsymbol{B}^{tr} \boldsymbol{X} + (\widetilde{S}, \mathcal{L}\widetilde{S}) \right), \tag{20}$$

to obtain the phase shifts by using the relation [23]

$$K_\ell = \tan \delta_\ell = (u_{01} + u_{11} L_\ell)(u_{00} + u_{10} L_\ell)^{-1}, \tag{21}$$

reintroducing the subscript ℓ.

C. PsH Bound State

As done earlier by Van Reeth and Humberston [21, 22], we use the short-range correlation part of the ^1S-wave scattering wavefunction to compute the binding energy, E_b, of the ^1S PsH system. This gives us some confidence of the reliability of using these short-range terms for the Ps-H scattering problem. The wavefunction we use for the bound state is

$$\Psi^+_{B.S.} = \sum_{i=1}^{N(\omega)} c^+_{i0} \bar{\phi}^+_{i01}, \tag{22}$$

where $\bar{\phi}^+_{i01}$ is given in Eq. (8) with $\ell = 0$.

D. Born-Oppenheimer Approximation

Using the first term, $\widetilde{S}_\ell$, in the wavefunction, Eqs. (1) and (2), for the Kohn variational method, $\bar{S}_\ell$, gives the Born-Oppenheimer (BO) approximation to $\tan\delta_\ell$, namely

$$\tan\delta^{BO}_\ell = -(\bar{S}_\ell, \mathcal{L}\bar{S}_\ell)\,. \tag{23}$$

E. Effective Range Theories

The scattering length [55] is defined as

$$a^\pm_\ell = -\lim_{\kappa\to 0} \frac{\tan\delta^\pm_\ell}{\kappa^{2\ell+1}}. \tag{24}$$

We consider the approximation with very small κ of

$$a^\pm_\ell \approx -\frac{\tan\delta^\pm_\ell}{\kappa^{2\ell+1}}. \tag{25}$$

To avoid confusion with the Bohr radius, a_0, we denote the S-wave scattering length $a_{\ell=0}$ as a.

For short-range interactions, the $^{1,3}S$-wave effective range theory (ERT) expansion is given by [70, 71]

$$\kappa\cot\delta^\pm_0 = -\frac{1}{a^\pm} + \frac{1}{2} r^\pm_0 \kappa^2, \tag{26}$$

where $r^\pm_0$ is the effective range. This ERT expansion has been used in the literature [21, 29, 42, 47] to compute the scattering length and effective range for Ps-H scattering. For the van

der Waals (vdW) interaction, which is the dominant long-range interaction between Ps and H [21, 72, 73], the scattering length is only defined for the S- and P-waves, and the effective range is defined for only the S-wave [74]. An S-wave ERT expansion for the van der Waals interaction is given in Ref. [75], which for Ps-H scattering where the mass of Ps is two, has the form

$$\kappa \cot \delta_0^{\pm} = -\frac{1}{a^{\pm}} + \frac{1}{2} r_0^{\pm} \kappa^2 - \frac{4\pi C_6}{15(a^{\pm})^2} \kappa^3 - \frac{16 C_6}{15 a^{\pm}} \kappa^4 \ln(\kappa) \,. \tag{27}$$

We use the van der Waals coefficient of $C_6 = 34.78473$ a.u., as given by Martin and Fraser [76].

Gao [77] has developed a quantum defect theory (QDT) for an attractive r^{-6} potential, obtaining an equation relating the tangent of the phase shifts to elements of a Z matrix (see Ref. [77]) and an analytic function of energy K_ℓ^0 [78]

$$\tan \delta_\ell = [Z_{ff} - K_\ell^0 Z_{gf}]^{-1} [K_\ell^0 Z_{gg} - Z_{fg}]. \tag{28}$$

K_ℓ^0 can be expanded in powers of the energy [78] of the incoming Ps atom as

$$K_\ell^0(E_{\boldsymbol{\kappa}}) = K_\ell^0(0) + K_\ell^{0\prime}(0) E_{\boldsymbol{\kappa}} + \ldots . \tag{29}$$

We retain the first two terms in the expansion and determine the coefficients $K_\ell^0(0)$ and $K_\ell^{0\prime}(0)$ by fitting the phase shifts to Eq. (29). We compute the $^{1,3}S$- and $^{1,3}P$ scattering lengths and $^{1,3}S$-wave effective ranges using the expressions given by Gao [78], which relates these quantities to the coefficients.

We also obtain an estimate of r_0^+ by using the following equation from Ref. [47]

$$r_0^+ = \frac{a^+ \sqrt{4E_b} - 1}{2 a^+ E_b}. \tag{30}$$

In this equation, we use our result of E_b and of a^+ that we obtain using Eq. (26) for the range $\kappa = 0.001 - 0.009$.

III. NUMERICS

We present briefly the numerical techniques below. Details can be found in Ref. [20].

A. Short-Short Integrations

For the ^1S PsH bound state and $^{1,3}S$ Ps(1s)-H(1s) elastic scattering calculations, we use the efficient asymptotic expansion method presented by Drake and Yan [27] for the evaluation of correlated integrals of the form

$$I(j_1, j_2, j_3, j_{12}, j_{23}, j_{31}; \bar{\alpha}, \bar{\beta}, \bar{\gamma}) = \int d\mathbf{r}_1 d\mathbf{r}_2 d\mathbf{r}_3 r_1^{j_1} r_2^{j_2} r_3^{j_3} r_{12}^{j_{12}} r_{23}^{j_{23}} r_{31}^{j_{31}} e^{-(\bar{\alpha} r_1 + \bar{\beta} r_2 + \bar{\gamma} r_3)} \,. \tag{31}$$

These integrals arise from evaluation of the matrix elements $(\bar{\phi}_{i\ell k}, \mathcal{L}\bar{\phi}_{j\ell k})$, $(\bar{\phi}_{i\ell k}, H\bar{\phi}_{j\ell k})$, and $(\bar{\phi}_{i\ell k}, \bar{\phi}_{j\ell k})$, where H is the full Hamiltonian given in Eqs. (10) and (11). The relationship between $\bar{\alpha}$ and α can be seen by considering these matrix elements, as can that of $\bar{\beta}$, β, $\bar{\gamma}$, γ, and the r_i and r_{ij} exponents. We also use the recursion relations of Pachucki et al. [79] to confirm the calculations of the short-range integrals for the S-wave and P-wave.

For $\ell > 0$, the short-range integrals have the form of

$$I(\ell_1' m_1', \ell_2' m_2', \ell_3' m_3'; j_1, j_2, j_3, j_{12}, j_{23}, j_{31}; \bar{\alpha}, \bar{\beta}, \bar{\gamma}) = \int d\mathbf{r}_1 d\mathbf{r}_2 d\mathbf{r}_3 r_1^{j_1} r_2^{j_2} r_3^{j_3} r_{12}^{j_{12}} r_{23}^{j_{23}} r_{31}^{j_{31}} \times e^{-(\bar{\alpha} r_1 + \bar{\beta} r_2 + \bar{\gamma} r_3)} Y^*_{\ell_1' m_1'}(\mathbf{r}_1) Y^*_{\ell_2' m_2'}(\mathbf{r}_2) Y^*_{\ell_3' m_3'}(\mathbf{r}_3) Y_{\ell_1 m_1}(\mathbf{r}_1) Y_{\ell_2 m_2}(\mathbf{r}_2) Y_{\ell_3 m_3}(\mathbf{r}_3) \,. \tag{32}$$

We solve these integrals using two different procedures. We use the procedure given by Van Reeth [61] for $\ell \leq 2$. In this procedure, we rotate and then integrate over external angles, reducing these integrals down to the form of Eq. (31), which we solve using the asymptotic expansion method [27]. This procedure requires separate derivations and codes for each partial wave. The other procedure we use is from Yan and Drake [28] and works for arbitrary ℓ, requiring only a single codebase. We present results using this procedure for only $\ell > 2$ due to its increased computational cost.

B. Long-Range Integrations

We evaluate the long-range–long-range and short-range–long-range matrix elements in the matrix equation $\boldsymbol{AX} = \text{-}\boldsymbol{B}$ using the standard Gauss-Laguerre and Gauss-Legendre quadratures. Due to cusps at $r_1 = r_2$ and $r_2 = r_3$ in the integrands, we split the r_2 and

r_3 integrations into Gauss-Legendre quadratures before each cusp and Gauss-Laguerre after each cusp. Ref. [68] discusses a similar type of cusp. Previous calculations [21, 22] treated these cusps as unimportant by 25 a.u., while we have extended it to 100 a.u. before we consider them unimportant. We find that this improves the convergence of the matrix elements.

To further improve the convergence of the short-range–long-range matrix elements, we note that the biggest source of difficulty comes from the Gauss-Laguerre quadratures in the r_1, r_2 and r_3 integrations – especially r_1. We increase the number of integration points to more than seven times as many as in previous work [21, 22] to better represent the integrands. We use a visual representation of the matrix elements to determine convergence using the Developer's Image Library [80]. The brute force approach of increasing the integration points can increase the computational time greatly, so we take another approach to further increase the accuracy. Specifically, the tails of the integrands are negligible, and the integrand closer to the origin is not represented adequately. To resolve this, for each of the Gauss-Laguerre quadratures, we introduce an extra $e^{-\lambda r_i}$, where i = 1, 2, 3, and remove it with $e^{\lambda r_i}$ after the quadrature, bringing the abscissae closer to the origin without increasing the number of integration points. We choose $\lambda = 1$.

C. Selection of Short-Range Terms

We use a method from Todd [26] to help remove short-range terms that contribute to linear dependence. This is a variation of the procedure from Lüchow and Kleindienst [81]. They use multiple blocks, while we optimize with a single block. They also use a criteria of ΔE to determine when to discard terms. Instead, we compare the lowest eigenvalues from the separate calculations using the upper and lower triangular matrices in LAPACK's `dsygv` routine [82], discarding terms when they cause the difference to be greater than a predetermined threshold.

We observe that using the terms selected by Todd's procedure allows us to use more short-range terms from the complete set before linear dependence occurs. The phase shifts are calculated using this set of short-range terms for the generalized Kohn variational method for multiple τ values in Eq. (7a). We further truncate this basis set where the phase shifts for the generalized Kohn variational method for different τ values begin to noticeably diverge, as

seen in Fig. 2, or when there is a significant jump in the phase shifts at high ω. This method with an appropriate choice of nonlinear parameters normally gives a reliable set of short-range terms, which we use to obtain the S-matrix complex Kohn results given in Sec. IV. For ^1S only, we also determine the truncation of the basis set by performing variations of μ (Eq. 6) [20]. For $\ell = 3$ at low κ, we use a restricted set of short-range terms where we eliminate terms with powers of $r_3 \geq 2$ if $\omega \geq 3$, improving the convergence ratios defined in Eq. (36) and giving more stable results [20, 21].

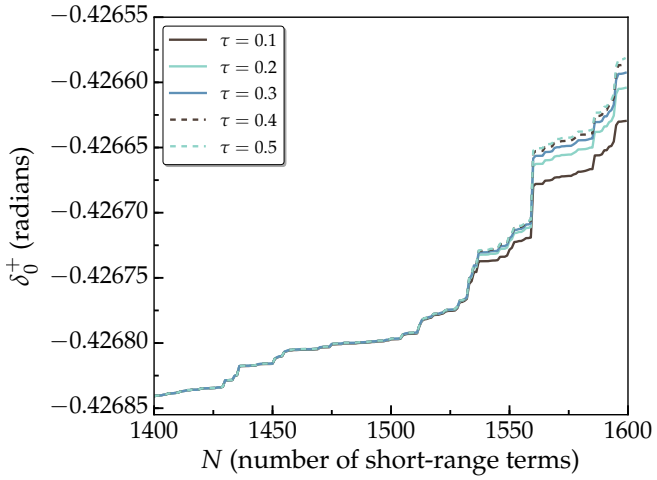

FIG. 2: (Color online) Breakdown in convergence of the ^1S phase shifts with respect to number of short-range terms for different τ values for the generalized Kohn variational method

We denote the number of short-range terms of a particular symmetry after we perform the possible truncations by $N'(\omega)$, where $N'(\omega) \leq N(\omega)$. The $N(\omega)$ of the wavefunctions given by Eqs. (1), (2), and (22) are replaced by $N'(\omega)$. When we perform convergence checks via extrapolations, we arrange the set of $N'(\omega)$ terms in the original ordering.

D. Fittings

As with the previous Kohn and inverse Kohn calculations [22], we fit our computed phase shifts near the resonances for ^1S and ^1P to the resonance formula

$$\delta(E_{\boldsymbol{\kappa}}) = A + BE_{\boldsymbol{\kappa}} + CE_{\boldsymbol{\kappa}}^2 + \arctan\left[\frac{^1\Gamma}{2(^1E_R - E_{\boldsymbol{\kappa}})}\right] + \arctan\left[\frac{^2\Gamma}{2(^2E_R - E_{\boldsymbol{\kappa}})}\right] \tag{33}$$

to extract out the positions (^1E_R and ^2E_R) and widths ($^1\Gamma$ and $^2\Gamma$) of the two resonances. This formula comprises the Breit-Wigner resonance terms [22, 83–85] for the two resonances and allows for a slowly varying polynomial background. We evaluate the resonance parameters for one resonance each for ^1D and ^1F, so we perform these fits without the second arctan term. We fit the data from the Kohn variational method and its variants (inverse Kohn, generalized Kohn, complex Kohn for the T matrix and complex Kohn for the S matrix) to determine the resonance parameters using the MATLAB [86] nonlinear fitting routine `nlinfit` with all eight possible weightings.

The Kohn variational method and variants of the method do not give rigorous lower bounds to the phase shifts, but they are found to give empirical bounds away from Schwartz singularities. We extrapolate the S-matrix complex Kohn phase shifts in Tables III, IV, V, and VI according to the empirical formula [21, 68]

$$\tan\delta_\ell^\pm(\omega) = \tan\delta_\ell^\pm(\omega\to\infty) + \frac{c}{\omega^p}, \tag{34}$$

where c and p depend on each extrapolation. For the $^{1,3}S$, $^{1,3}P$ and ^1D phase shifts, we use these extrapolated values to estimate the convergence of the phase shifts and the error in the final results, which we report in Sec. IV B. We use a similar procedure to extrapolate the $^{1,3}S$- and $^{1,3}P$-wave scattering lengths by fitting to the empirical formula [21]

$$a_\ell^\pm(\omega) = a_\ell^\pm(\omega\to\infty) + \frac{d}{\omega^q}, \tag{35}$$

where d and q depend on each extrapolation. The percent difference between the scattering length at $\omega = 7$ and the extrapolated scattering length is considered the error in Tables XI and XII. We see no convergence pattern for the effective range.

For $\ell \geq 2$, we experience difficulty in extrapolating phase shifts using Eq. (34). To determine whether the phase shifts are converging with respect to ω, we compute a convergence ratio defined as

$$R'(\omega) = \frac{\delta_\ell^\pm(\omega) - \delta_\ell^\pm(\omega-1)}{\delta_\ell^\pm(\omega-1) - \delta_\ell^\pm(\omega-2)}, \tag{36}$$

where $R'(\omega)$ depends on ℓ and whether we are considering the singlet or triplet. This is similar to the inverse of the ratio for the energy eigenvalues given in Ref. [30]. We find that if $R'(\omega) \lesssim 0.5$, we can typically obtain extrapolated phase shifts with some degree of reliability. In contrast, if $R'(\omega) \geq 1$, there is no convergence pattern and thus we would not be confident with extrapolated phase shifts.

E. Nonlinear Parameters and Terms in the Scattering Wavefunctions

Partial wave	ω	$N'(\omega)$	α	β	γ	μ	m_ℓ
^1S	7	1505	0.568	0.580	1.093	0.9	1
^3S	7	1633	0.323	0.334	0.975	0.9	1
^1P	7	1000	0.397	0.376	0.962	0.9	3
^3P	7	1000	0.310	0.311	0.995	0.9	3
^1D ($\kappa < 0.3$)	6	916	0.359	0.368	0.976	0.7	7
^1D ($\kappa \geq 0.3$)	6	913	0.600	0.368	0.976	0.7	7
^3D ($\kappa < 0.3$)	6	919	0.356	0.365	0.976	0.7	7
^3D ($\kappa \geq 0.3$)	6	913	0.600	0.365	0.976	0.7	7
^1F ($\kappa < 0.4$)	5	385*	0.359	0.368	0.976	0.7	7
^1F ($\kappa \geq 0.4$)	5	462	0.500	0.600	1.100	0.7	7
^3F ($\kappa < 0.4$)	5	385*	0.356	0.365	0.976	0.7	7
^3F ($\kappa \geq 0.4$)	5	462	0.600	0.365	0.976	0.7	7
^1G ($\kappa < 0.45$)	5	462	0.359	0.368	0.976	0.7	9
^1G ($\kappa \geq 0.45$)	5	462	0.500	0.600	1.100	0.7	9
^3G ($\kappa < 0.45$)	5	462	0.356	0.365	0.976	0.7	9
^3G ($\kappa \geq 0.45$)	5	462	0.600	0.365	0.976	0.7	9
^1H ($\kappa < 0.5$)	5	462	0.359	0.368	0.976	0.7	11
^1H ($\kappa \geq 0.5$)	5	462	0.500	0.600	1.100	0.7	11
^3H ($\kappa < 0.45$)	5	462	0.356	0.365	0.976	0.7	11
^3H ($\kappa \geq 0.45$)	5	462	0.600	0.365	0.976	0.7	11

TABLE I: Nonlinear parameters α, β, γ, μ, integer power m_ℓ in the shielding function, ω, and the number of terms $N'(\omega)$ of each symmetry in the wavefunction for each partial wave. Numbers marked with a star indicate the restriction in the r_3 power described in Sec. III C.

Table I shows the number of terms for each short-range symmetry, $N'(\omega)$, used for each partial wave. The wavefunction for the S-wave uses a total of $N'(\omega)$ short-range terms, and the wavefunction for the higher partial waves use a total of $2N'(\omega)$ short-range terms, as given by Eqs. (1) and (2) with the $N(\omega)$ replaced by $N'(\omega)$. For the first three partial

waves, we use Todd's procedure described in Sec. III C. This table also gives the value of ω, the parameters α, β, and γ in Eq. (8), and the parameters μ and m_ℓ in Eq. (6) used for each partial wave.

For $\ell \geq 2$, where we have neglected the mixed symmetry terms, we find that the phase shifts are more sensitive to the choice of nonlinear parameters α, β, and γ than for the $^{1,3}S$- and $^{1,3}P$-waves. We also find that for $\ell \geq 2$, the triplet is more sensitive than the singlet. The optimum choice of these of nonlinear parameters appears to be κ-dependent. For $\ell \geq 2$, we use two different sets of these nonlinear parameters.

IV. RESULTS

A. Bound State Results

We use the ^1S PsH bound state results as a measure of the reliability of the short-range part of the wavefunction to describe ^1S Ps-H scattering at small distances. The Rayleigh-Ritz variational method provides a true upper bound on the total energy, which converges well with respect to ω. We report the results of the total and binding energies we obtain with the same set of nonlinear parameters α, β, and γ and the same number of terms $N'(7)$ that we use in the scattering calculation and which we give in Table I. Table II compares the energies for the ^1S PsH bound state that we obtain with $\omega = 7$ (1505 terms) with the results from other groups.

Our calculation yields a better value for the binding energy than the earlier variational calculations of Refs. [21, 22] but not as good as the variational calculation of Ref. [30], which also used Hylleraas-type functions. While we do not obtain the best value of the binding energy, the result we obtain for this quantity compares favorably with the most elaborate calculation in the literature, which used 5000 ECGs [36]. Our calculation of the binding energy gives us some confidence in the reliability of the short-range part of the scattering wavefunction to describe the ^1S Ps-H scattering system.

B. Phase Shifts and Cross Sections

In Tables III and IV, we show the $^{1,3}S$ phase shifts using the S-matrix complex Kohn variational method. After removing any obvious Schwartz singularities, the results from the

Method	Terms	E (a.u.)	E_b (eV)
Current work ($\omega = 7$)	1505	−0.789 189 725	1.066 406 705
Variational Hylleraas ($\omega = 6$) [21]	721	−0.789 156	1.065 5*
Variational Hylleraas [34]	396	−0.788 945*	1.059 75
Variational Hylleraas ($\omega \to \infty$) [30]	—	−0.789 196 714 7*	1.066 596 896
CC 14Ps14H [47]	—	−0.786 5	0.994*
CC 14Ps14H + H^- [29]	—	−0.787 9	1.03*
ECGs with SVM [35]	1800	−0.789 196 740*	1.066 597 58
ECGs variational [36]	5000	−0.789 196 765 251*	1.066 598 271 959

TABLE II: PsH total energy, E, and binding energy, E_b, comparisons. The values marked with a star are the reported values, and the other values are obtained by using the conversion factor given in Ref. [59].

Kohn variational method and its variants described in Sec. II B (Kohn, inverse Kohn, generalized Kohn, T-matrix complex Kohn, and S-matrix complex Kohn) agree to the accuracy given. We use Eq. (34) and the phase shifts for $\omega = 4$ to 7 to compute extrapolated phase shifts for $\omega \to \infty$. By computing the percentage difference between the extrapolated phase shifts and the computed phase shifts at $\omega = 7$, we estimate that the ^1S phase shifts have converged to better than about 0.22% for the range $\kappa = 0.1$ to 0.7 and that the ^3S phase shifts have converged to better than 0.27% for the same range of κ.

In these tables, we compare the S-matrix complex Kohn results with the earlier variational results [21, 22] and with the elaborate CC results of Refs. [29, 47]. The current $\omega = 7$ results are in excellent agreement with the earlier Kohn and inverse Kohn $\omega = 6$ variational results, being either identical or slightly lower, indicating that the earlier S-wave results were well-converged. The slight difference in phase shifts between the previous Kohn/inverse Kohn and the present complex Kohn calculation can be attributed to at least the following factors. Using Todd's procedure (described in Sec. III C) allows us to use more terms (see Table I) than the earlier Kohn and inverse Kohn calculations [21, 22], which used 721 terms. Using the asymptotic expansion also allows us to use more short-range terms. The increase in the number of short-range terms slightly increases the phase shifts, but we also use more integration points in these calculations, which can also change the phase shifts.

The complex Kohn results are in good agreement with the CC results of the Walters' group [29, 47]. For the singlet, the complex Kohn phase shifts are slightly larger than the

CC results. In general, because of the empirical bounds on the complex Kohn results and, in practice on the CC [47], the complex Kohn results could be slightly more accurate than the CC. However, for the triplet, the Kohn results are slightly more negative than the CC results.

The recent CVM S-wave results from Zhang and Yan [58] agree extremely well with the complex Kohn results, even for the triplet. In Fig. 3, we compare the $^{1,3}S$ phase shifts we obtain from the complex Kohn variational method with results from various other calculations. Figure 4(a) compares the complex Kohn phase shifts over the energy range up to the Ps(n=2) threshold with the CC and CVM results. The inset in this figure shows the small discrepancy with the CC phase shifts, but excellent agreement between the three sets of results is evident.

Tables V and VI give the $^{1,3}P$ and $^{1,3}D$ phase shifts that we determine using the S-matrix complex Kohn variational method. The small percentage differences with the extrapolated values for the $^{1,3}P$-waves indicate that the complex Kohn phase shifts are well converged. The complex Kohn ^1P phase shifts are above the CC results, whereas the complex Kohn ^3P phase shifts are generally slightly below. Figure 4(b) shows that the complex Kohn and CC results agree relatively well. From Table VI, the ^3D phase shifts are positive for lower κ but become negative for higher κ. It is noted in Ref. [47] that this behavior shows that the interaction is repulsive for low κ and attractive for higher κ.

We have difficulty performing extrapolations on the $^{1,3}D$ phase shifts. For ^1D, the $\kappa = 0.1$ extrapolation is not reliable, and the percentage difference is correspondingly large, even though the convergence ratio $R'(6)$ given by Eq. (36) is less than 1. As seen in Table VI, for $\kappa = 0.2$, the percentage difference between the ^1D extrapolated phase shift and the $\omega = 6$ phase shift is about 6%, whereas in the range $\kappa = 0.3 - 0.7$, the percentage difference is less than 2%. The percentage difference for ^3D is larger than for ^1D, and thus there is less confidence in the ^3D extrapolated phase shifts (which we do not include in Table VI). The larger percentage difference for the triplet than the singlet could be a reflection that the mixed symmetry terms are more important for the triplet than for the singlet. If this is the case, this would be an interesting finding, since for e^--H scattering, the mixed symmetry terms were found to be more important for the singlet than for the triplet [69]. Inclusion of the mixed symmetry terms for Ps-H scattering for $\ell \geq 2$ should be investigated.

The $\omega = 5$ and $\omega = 6$ phase shifts differ by no more than 10% for ^1D. For ^3D, this

difference is up to 24% for $\kappa = 0.3$ but much less for other κ values, down to about 4% for $\kappa = 0.7$. The percentage difference between the ^3D-wave $\omega = 6$ and extrapolated phase shifts for $\kappa = 0.1$ is very large, $\approx 140\%$, but this difference for the range $0.2 - 0.7$ is less than 25%, except for $\kappa = 0.4$, where the percentage difference is larger at 40%. We note that between $\kappa = 0.3$ and 0.4, the complex Kohn ^3D phase shifts change from positive to negative.

The S-matrix complex Kohn $^{1,3}D$ phase shifts are generally below the corresponding CC phase shifts, as can be seen in Table VI and Fig. 4(c). However, the extrapolated ^1D phase shifts are slightly larger than the CC phase shifts at both $\kappa = 0.6$ and 0.7. Fig. 4(c) shows that the overall shape of the complex Kohn phase shift curves is similar to the CC. However, the percentage difference between the CC and complex Kohn ^1D phase shifts is about 39% at low κ and decreases to less than 1% for higher κ (not including the resonance region of $\kappa > 0.7$ or $E_{\boldsymbol{\kappa}} > 3.3$ eV). The larger discrepancy comes with the ^3D phase shifts, which have a percentage difference between the CC and the complex Kohn of over 30%, often much larger, through the entire energy range. We note that the percentage differences with the CC results for ^3P are also large at lower κ values. For ^3P with $\kappa \geq 0.01$, where there are no mixed symmetry terms to neglect, we do not face the convergence and extrapolation difficulties we have for ^3D.

The ^3D phase shifts are small, and their contribution to the elastic integrated cross section is correspondingly small. Before the resonance region ($\kappa \leq 0.7$ or $E_{\boldsymbol{\kappa}} < 3.3$ eV), the ^1D and ^3D partial waves contribute up to 6.6% and 0.53% to the elastic integrated cross section, respectively. In the full energy range we consider, including the resonance region, the ^3D-wave contributes a maximum of 1.34%. We notice no appreciable difference to the elastic integrated cross section when the complex Kohn $^{1,3}D$ phase shifts are replaced by the CC $^{1,3}D$ phase shifts (less than 0.084%). The triplet D-, F-, G-, and H-wave phase shifts are more sensitive to the nonlinear parameters α, β, and γ than the singlet, but in general, the triplet contribution to the elastic differential and integrated cross sections are less than the corresponding singlet contribution.

κ (a.u.)	$\delta_0^+(\omega=7)$	$\delta_0^+(\omega\to\infty)$	% Diff$^+$	δ_0^+ (Kohn) [21]	δ_0^+ (CC 14Ps14H+H$^-$) [29]	δ_0^+ (CVM) [58]
0.1	−0.427	−0.426	0.223%	−0.427	−0.428	−0.42629
0.2	−0.820	−0.819	0.010%	−0.820	−0.825	−0.81973
0.3	−1.161	−1.161	0.040%	−1.161	−1.167	—
0.4	−1.446	−1.446	0.022%	−1.446	−1.453	—
0.5	−1.678	−1.677	0.031%	−1.677	−1.685	—
0.6	−1.858	−1.857	0.040%	−1.857	−1.867	—
0.7	−1.964	−1.963	0.045%	−1.964	−1.992	—

TABLE III: ^1S phase shifts for Ps-H scattering. δ_0^+ are the current S-matrix complex Kohn phase shifts, and % Diff$^+$ is the percent difference between the complex Kohn $\omega = 7$ and $\omega \to \infty$ results.

κ (a.u.)	$\delta_0^-(\omega=7)$	$\delta_0^-(\omega\to\infty)$	% Diff$^-$	δ_0^- (Kohn) [21]	δ_0^- (CC 14Ps14H) [47]	δ_0^- (CVM) [58]
0.1	−0.215	−0.214	0.120%	−0.215	−0.206	−0.21461
0.2	−0.431	−0.431	0.063%	−0.432	−0.414	−0.43145
0.3	−0.645	−0.645	0.094%	−0.645	−0.624	—
0.4	−0.850	−0.849	0.130%	−0.850	−0.838	—
0.5	−1.041	−1.040	0.166%	−1.040	−1.037	—
0.6	−1.217	−1.214	0.273%	−1.215	−1.213	—
0.7	−1.375	−1.372	0.250%	−1.373	−1.367	—

TABLE IV: ^3S phase shifts for Ps-H scattering. δ_0^- are the current S-matrix complex Kohn phase shifts, and % Diff$^-$ is the percent difference between the current complex Kohn $\omega = 7$ and $\omega \to \infty$ results.

κ (a.u.)	$\delta_1^+(\omega=7)$	$\delta_1^+(\omega\to\infty)$	% Diff$^+$	δ_1^+ (CC 9Ps9H+H$^-$) [29]	$\delta_1^-(\omega=7)$	$\delta_1^-(\omega\to\infty)$	% Diff$^-$	δ_1^- (CC 9Ps9H) [47]
0.1	0.226^{-1}	0.227^{-1}	0.465%	0.221^{-1}	-0.178^{-2}	-0.172^{-2}	3.176%	-0.953^{-3}
0.2	0.191	0.192	0.306%	0.183	-0.167^{-1}	-0.165^{-1}	0.993%	-0.122^{-1}
0.3	0.609	0.611	0.314%	0.580	-0.552^{-1}	-0.540^{-1}	0.749%	-0.456^{-1}
0.4	0.994	0.996	0.205%	0.956	−0.115	−0.114	0.698%	−0.104
0.5	1.140	1.142	0.140%	1.106	−0.183	−0.182	0.749%	−0.178
0.6	1.162	1.163	0.137%	1.134	−0.248	−0.246	0.896%	−0.247
0.7	1.152	1.154	0.181%	1.133	−0.292	−0.288	1.230%	−0.295

TABLE V: $^{1,3}P$ phase shifts for Ps-H scattering. $\delta_1^\pm$ are the current S-matrix complex Kohn phase shifts, and % Diff$^\pm$ is the percent difference between the current complex Kohn $\omega = 7$ and $\omega \to \infty$ results. Powers of 10 are denoted by exponents.

κ (a.u.)	$\delta_2^+(\omega=6)$	$\delta_2^+(\omega\to\infty)$	% Diff$^+$	δ_2^+ (CC 9Ps9H+H$^-$) [29]	$\delta_2^-(\omega=6)$	δ_2^- (CC 9Ps9H) [47]
0.1	1.36^{-4}	—	—	2.02^{-4}	5.81^{-5}	8.48^{-5}
0.2	2.99^{-3}	3.18^{-3}	6.27%	3.49^{-3}	7.12^{-4}	1.15^{-3}
0.3	1.60^{-2}	1.62^{-2}	1.54%	1.73^{-2}	1.10^{-3}	2.84^{-3}
0.4	4.98^{-2}	5.04^{-2}	1.33%	5.22^{-2}	-1.80^{-3}	2.37^{-3}
0.5	1.13^{-1}	1.14^{-1}	1.52%	1.16^{-1}	-1.07^{-2}	-4.66^{-3}
0.6	2.06^{-1}	2.09^{-1}	1.67%	2.08^{-1}	-2.54^{-2}	-1.85^{-2}
0.7	3.28^{-1}	3.33^{-1}	1.67%	3.24^{-1}	-4.28^{-2}	-3.27^{-2}

TABLE VI: $^{1,3}D$ phase shifts for Ps-H scattering. $\delta_2^\pm$ are the current S-matrix complex Kohn phase shifts, and % Diff$^+$ is the percent difference between the current complex Kohn $\omega = 6$ and $\omega \to \infty$ results. Powers of 10 are denoted by exponents.

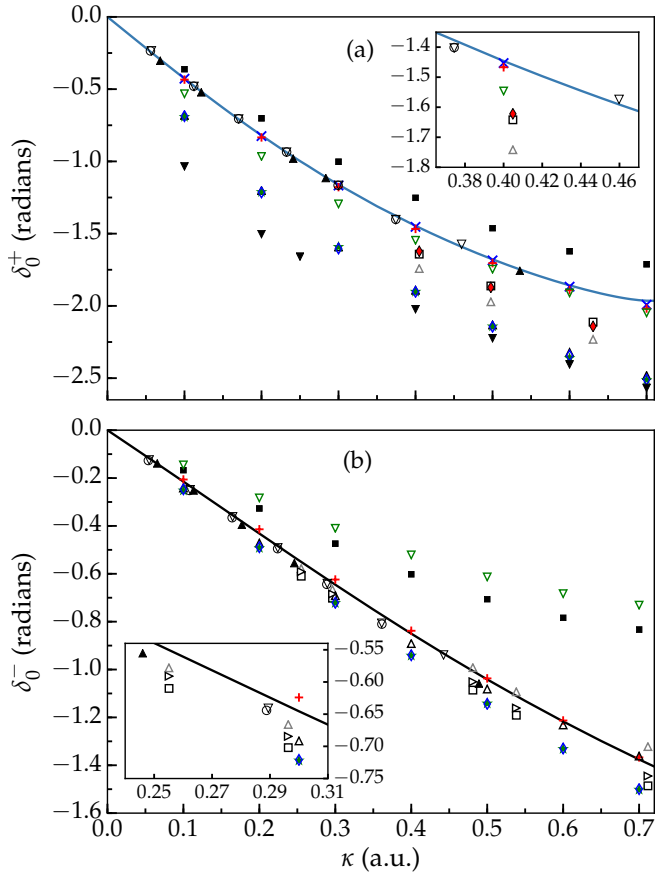

FIG. 3: (Color online) Comparison of ^1S (a) and ^3S (b) S-matrix complex Kohn phase shifts with results from other groups. The insets show a magnified portion of the same data for each. Results are ordered according to year of publication. References marked with an asterisk have values extracted from figures in their work. Solid curves – this work; × – CC [29]; ● – Kohn [21]; + – CC [47]; ▲ – DMC* [40]; ▽ – SVM 2002* [42]; ○ – SVM 2001* [41]; ▽ – 2 channel / static exchange with model exchange [87]; △ – 6-state CC [46]; ■ – 5-state CC [45]; □ – Coupled pseudostate [44]; △ – 3-state CC [43]; ★ – Static exchange [50]; ▷ – Stabilization [39]; ♦ – Stabilization [38]; ◊ – Static exchange [49]; ▼ – Static exchange [88].

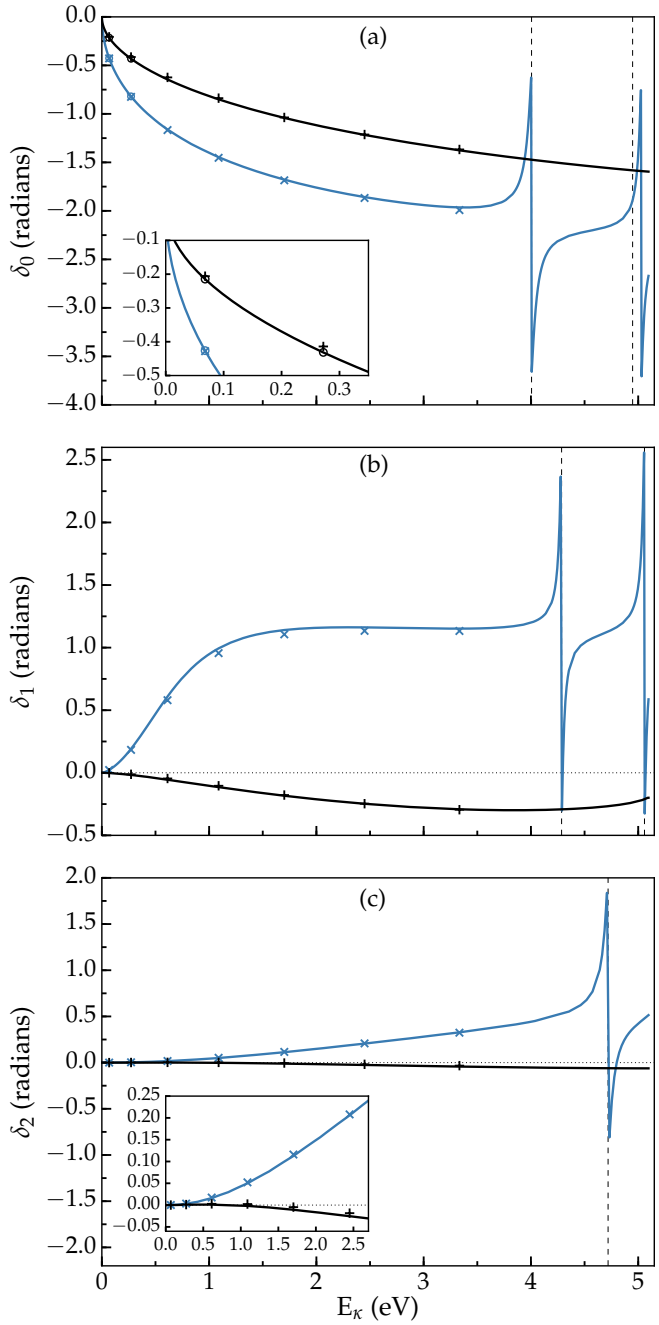

FIG. 4: (Color online) Phase shifts for Ps-H scattering: (a) S-wave; (b) P-wave; (c) D-wave. Insets in (a) and (c) show a zoomed in view of the low-energy regions. Current singlet and triplet S-matrix complex Kohn phase shifts are the solid blue (dark gray) and black, respectively. The singlet CC phase shifts [29] are given by $\times$, and the triplet CC phase shifts [47] are given by $+$. The CVM ^1S- and ^3S-wave phase shifts [58] are blue (dark gray) and black circles, respectively. Vertical dashed lines denote the complex rotation resonance positions [30–32].

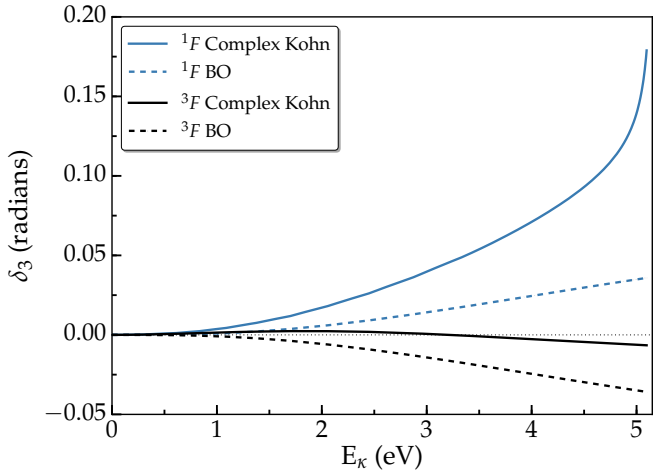

FIG. 5: (Color online) F-wave phase shifts for Ps-H scattering. Singlet phase shifts are given in blue (dark gray), and triplet phase shifts are black. This figure compares the complex Kohn phase shifts with the BO approximation phase shifts.

Figure 5 shows the F-wave complex Kohn phase shifts compared to the BO phase shifts that we compute. As for the ^3D, there is a sign change from positive to negative for the ^3F phase shifts, but this change occurs at a higher energy of approximately 3.2 eV. The ^1F-wave has a resonance above the Ps(n=2) threshold, but the beginning of the resonance is evident in Fig. 5. The difference between the ^1F phase shifts for $\omega = 4$ and 5 is less than 10% for $\kappa \geq 0.5$ (1.7 eV). The corresponding difference for the ^3F phase shifts is greater than 50%, however the triplet contributes much less to the elastic integrated cross section.

The BO approximation phase shifts do not agree well with the complex Kohn phase shifts, being much lower. We also find little agreement between the BO phase shifts and the complex Kohn phase shifts for the $^{1,3}G$-wave and $^{1,3}H$-wave. In computing the elastic integrated cross sections, we would not be comfortable using the BO phase shifts for $\ell > 5$.

We perform complex Kohn calculations on all first six partial waves, but we do more elaborate calculations for the first three partial waves, as shown by the short-range terms used in Sec. III E. The ^3D, $^{1,3}F$, $^{1,3}G$, and $^{1,3}H$ partial waves are not fully converged, but for each of these, the phase shifts and elastic partial cross sections become very small, so they do not contribute much to the elastic integrated cross section. For the G- and H-waves, we obtain a convergence ratio $R'(5) > 1$ for $\kappa \leq 0.3$ and $\kappa \leq 0.35$, respectively, due to the very small phase shifts (on the order of $\lesssim 10^{-5}$) and probably the neglect of the mixed symmetry terms. The convergence ratios are less than 1 at higher κ, where there is a more significant

contribution to the elastic differential cross section. The maximum H-wave contribution to the elastic integrated cross section is 0.009% and much less at energies before the Ps(n=2) threshold.

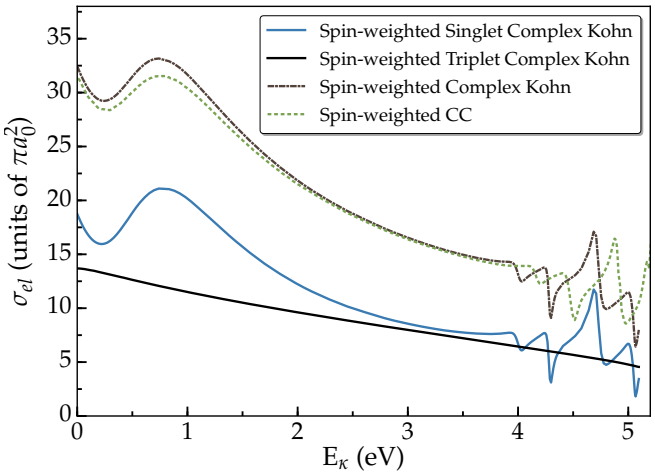

FIG. 6: (Color online) Elastic integrated cross sections. The singlet and triplet cross sections are weighted by 1/4 and 3/4, respectively. CC data is from Ref. [29]. We extract the CC data using the CurveSnap program [89].

Assuming that the initial spin state of the H(1s) target is unpolarized and that the spin final states are not determined, the spin-weighted cross sections (elastic differential, elastic integrated and momentum transfer) comprise of 1/4 of the singlet and 3/4 of the triplet corresponding cross sections [47, 50, 90]. We include partial waves with $\ell \leq 5$ for each of the cross sections. In Fig. 6, we show the complex Kohn spin-weighted singlet, spin-weighted triplet and the spin-weighted integrated cross sections for elastic scattering and which we compare with the corresponding spin-weighted CC results. There is good agreement between the complex Kohn and CC spin-weighted integrated elastic cross section for much of the energy range, but there is a clear shift in the positions of the resonances, which can also be seen in Tables VII, VIII, and IX. There is also some noticeable discrepancy at low $E_{\boldsymbol{\kappa}}$, which is especially noticeable near the maximum and minimum.

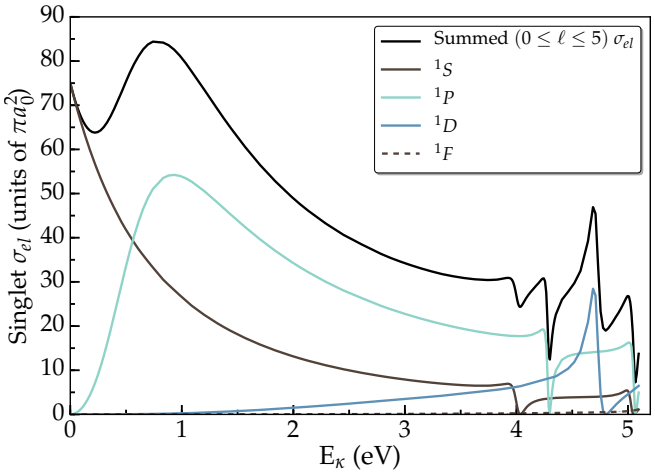

FIG. 7: (Color online) Singlet elastic partial wave cross sections and summed singlet elastic integrated cross section

It is interesting to note in Fig. 6 that the triplet elastic integrated cross section is nearly featureless, decreasing monotonically. The singlet cross section not only has resonance features but also exhibits a minimum at 0.25 eV and a maximum at 0.74 eV. The source of this minimum can be seen in Fig. 7 as a mixing of the ^1S and ^1P partial cross sections, and the maximum is due primarily to the ^1P.

The elastic differential cross section, calculated using the expression in Ref. [55], is shown in Figs. 8, 9, and 10. The percent difference by including the H-wave in the differential cross section compared to including through the G-wave is a maximum of 3.8% at higher $E_{\boldsymbol{\kappa}}$ but only an average of 0.26% throughout the full $E_{\boldsymbol{\kappa}}$ and θ ranges, indicating that the differential cross section is relatively well converged. Fig. 8 shows that the differential cross section is essentially isotropic at very low incident energy and becomes slightly more backward peaked as the energy is increased up to about 0.46 eV ($\kappa = 0.26$). However, around this energy, there is an abrupt change in the differential cross section. Backward scattering is reduced, and there is a rapid rise in the forward direction, reaching a maximum around 1 eV ($\kappa = 0.38$). There is little change in the behavior of the differential cross section going from $\kappa = 0.6$ (2.4 eV) to $\kappa = 0.7$ (3.3 eV). Also of interest is the angular dependence of the resonances shown in Figs. 9 and 10, for which we find that the main contribution is also forward peaked with some presence at large angles and little contribution at $\pi/2$. Interestingly, the structures discussed above are seen to arise principally from the singlet contribution.

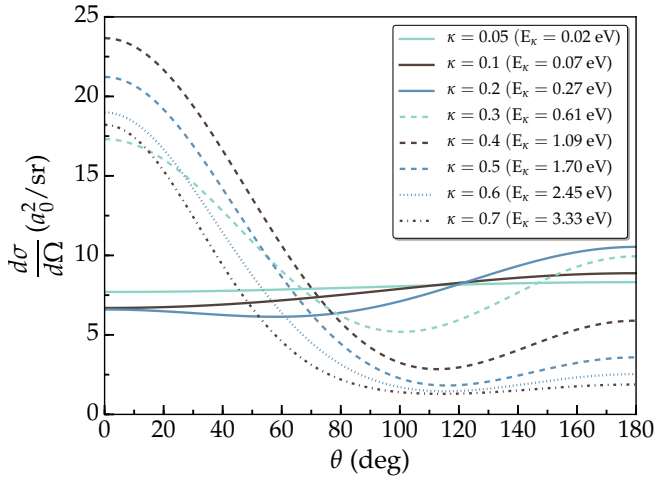

FIG. 8: (Color online) The elastic differential cross section for Ps-H scattering vs. scattering angle θ at selected incident Ps momenta (energy)

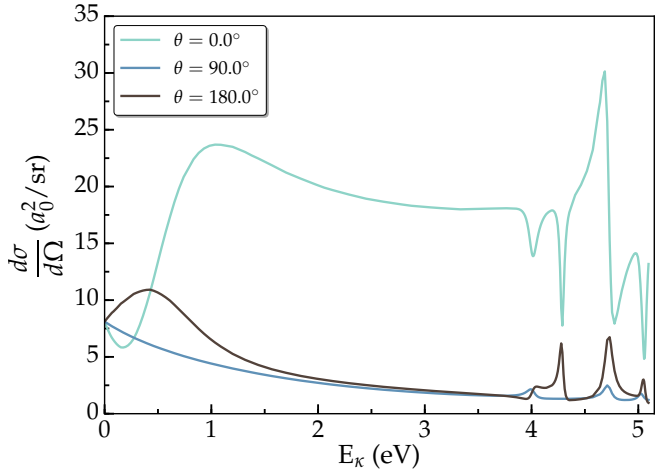

FIG. 9: (Color online) The elastic differential cross section for Ps-H scattering vs. energy of the incident Ps at selected angles

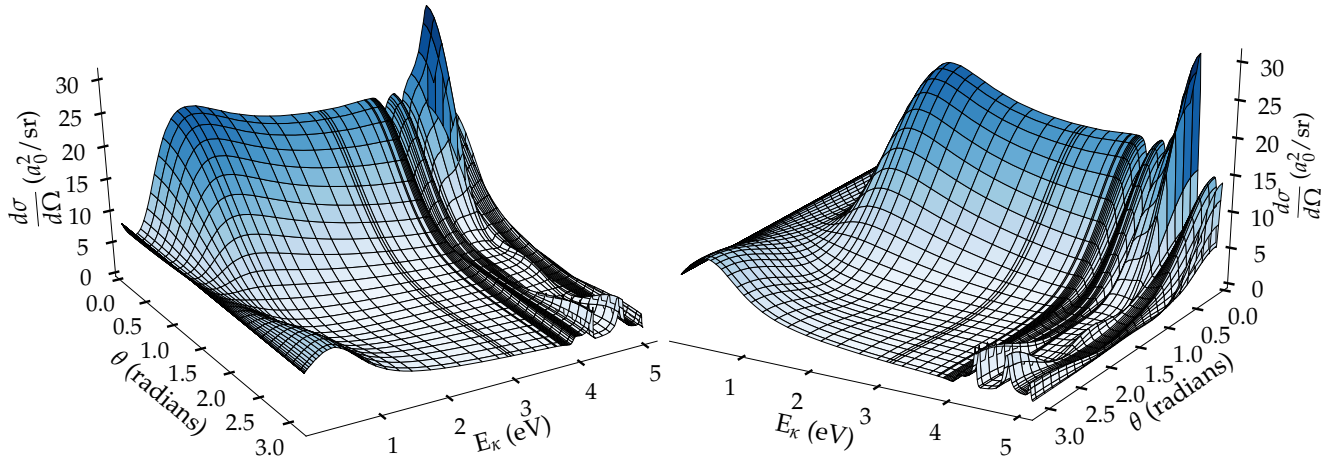

FIG. 10: (Color online) The elastic differential cross section for Ps-H scattering for two different rotations

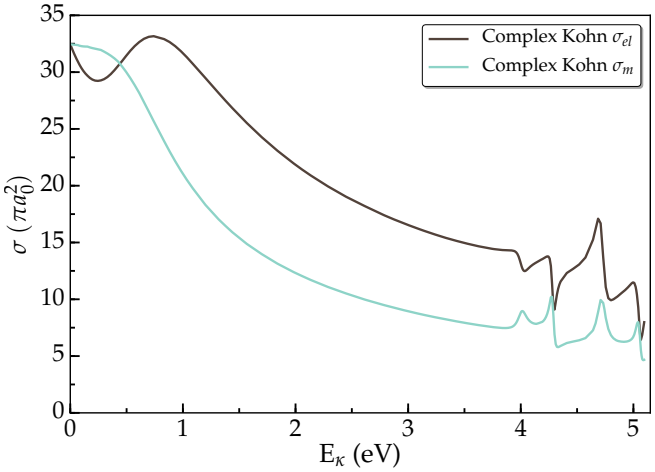

FIG. 11: (Color online) Comparison of cross sections. The complex Kohn integrated elastic cross section, σ_{el}, is given by the black curve. The complex Kohn momentum transfer cross section, σ_m, is given by the light blue (light gray) curve.

The momentum transfer cross section, σ_m, can be useful in plasma applications [91, 92]. These cross sections have been measured for Ps scattering with multiple atomic and molecular targets [93–95] and calculated for Ps scattering by inert gases [96]. Equations for σ_m are given in Refs. [55, 97]. In Fig. 11, we compare σ_m with σ_{el}, both of which we compute using the S-matrix complex Kohn phase shifts. For energies close to zero, $\sigma_m \approx \sigma_{el} \approx 32.45$ πa_0^2. The elastic differential cross section is isotropic at zero energy and almost isotropic

at very low energy (see Ref. [96] and Figs. 8 and 10). After zero energy, the momentum transfer cross section differs from the elastic integrated cross section. For the energy range $0 < E_{\boldsymbol{\kappa}} \lesssim 0.46$ eV, $\sigma_m > \sigma_{el}$, which indicates that the scattering is larger in the backward direction, as seen in Fig. 9. Above approximately 0.46 eV, the scattering becomes forward peaked, and $\sigma_m < \sigma_{el}$.

C. Resonances

The ^1S and ^1P partial waves each have two resonances below the Ps(n=2) threshold, and the ^1D has one resonance before. There is a resonance just above the threshold for ^1F, with the onset of the resonance obvious below the threshold. Drachman [98] concluded that these Rydberg resonances correspond to the quasibound state of e^+ with the H^- ion. Figure 4(a) shows the two ^1S Rydberg resonances below the Ps(n=2) threshold. The first resonance was first calculated by Hazi and Taylor using a stabilization method [99]. Their properties have been computed accurately by Yan and Ho using the complex rotation method [30] and by Walters' group using the CC approach [29].

We fit the phase shifts in the resonance region to Eq. (33) for ^1S and ^1P. We perform the ^1D and ^1F resonance fits without the second arctan term, since we consider only one resonance for each of these partial waves. In Tables VII, VIII, IX, and X, we compare the S-matrix complex Kohn resonance parameters with results from other calculations. We also give in these tables the average positions and widths we obtain using the Kohn variational method and its variants (inverse Kohn, generalized Kohn, complex Kohn for the T matrix and complex Kohn for the S matrix) after we remove the Schwartz singularities. We determine the standard deviation and use that for the errors.

The resonance parameters of the present S-matrix complex Kohn calculations agree well with those of the earlier Kohn/inverse Kohn calculations [22]. Also, the resonance parameters we obtain using the S-matrix complex Kohn phase shifts generally agree well with those obtained in the complex rotation calculations [30–33]. We see that there is more discrepancy between the complex Kohn and complex rotation calculations [30, 31] of the second ^1S- and ^1P-wave resonances than of the first. The resonance parameters we obtain using the S-matrix complex Kohn variational method are generally comparable to the CC results [29]. The ^1F resonance lies above the Ps(n=2) threshold, but we are able to fit the onset

of the resonance shortly before the threshold. The resonance parameters for ^1D and ^1F are particularly sensitive to the choice of nonlinear parameters α, β, and γ, and the estimation of the errors of these resonance parameters does not include this sensitivity.

We observe no triplet resonances for any of these partial waves, which is consistent with the discussion by Campbell et al. [44], who explained this result. However, we note that Ray [100] obtained a triplet resonance in a 3-state CC approximation.

Van Reeth and Humberston [22] found that for this system, a stabilization plot for ^1S predicted the first resonance position relatively well, but they could not obtain a resonance position as accurately as when they performed a scattering calculation. We use the same stabilization technique for the ^1S, ^1P, and ^1D partial waves and see a similar result to this previous work for ^1S. For ^1P and ^1D, if only the first symmetry is used, the eigenvalue positions do not line up well with the resonance positions determined from the full calculations in Tables VIII and IX. If both the first and second symmetries are used pairwise, the eigenvalues agree with the resonance positions from these tables. This seems to indicate that the mixed symmetry terms with shared angular momentum will probably not contribute much for ^1D. This analysis cannot be done with the triplet states, as they have no resonances.

Method	^1E_R (eV)	$^1\Gamma$ (eV)	^2E_R (eV)	$^2\Gamma$ (eV)
Current work: Average ± standard deviation	4.0065 ± 0.0001	0.0955 ± 0.0001	5.0272 ± 0.0029	0.0608 ± 0.0007
Current work: S-matrix complex Kohn	4.0065	0.0955	5.0278	0.0608
Complex rotation (Yan and Ho 1999) [30]	4.0058 ± 0.0005	0.0952 ± 0.0011	4.9479 ± 0.0014	0.0585 ± 0.0027
Stabilization (Yan and Ho 2003) [101]	4.007	0.0969	4.953	0.0574
Kohn variational (Van Reeth and Humberston 2004) [22]	4.0072 ± 0.0020	0.0956 ± 0.010	5.0267 ± 0.0020	0.0597 ± 0.0010
CC (Walters et al. 2004) [29]	4.149	0.103	4.877	0.0164

TABLE VII: ^1S resonance parameters for Ps-H scattering

Method	^1E_R (eV)	$^1\Gamma$ (eV)	^2E_R (eV)	$^2\Gamma$ (eV)
Current work: Average ± standard deviation	4.2856 ± 0.0001	0.0445 ± 0.0001	5.0577 ± 0.0004	0.0459 ± 0.0005
Current work: S-matrix complex Kohn	4.2856	0.0445	5.0579	0.0459
Complex rotation (Yan and Ho 1998) [31]	4.2850 ± 0.0014	0.0435 ± 0.0027	5.0540 ± 0.0027	0.0585 ± 0.0054
Stabilization (Yan and Ho 2003) [101]	4.287	0.0446	5.062	0.0563
Kohn (Van Reeth and Humberston 2004) [22]	4.29 ± 0.01	0.042 ± 0.005	—	—
CC (Walters et al. 2004) [29]	4.475	0.0827	4.905	0.0043

TABLE VIII: ^1P resonance parameters for Ps-H scattering

Method	^1E_R (eV)	$^1\Gamma$ (eV)
Current work: Average ± standard deviation	4.720 ± 0.001	0.0908 ± 0.0010
Current work: S-matrix complex Kohn	4.720	0.0909
Complex rotation (Ho and Yan 1998) [32]	4.710 ± 0.0027	0.0925 ± 0.0054
Stabilization (Yan and Ho 2003) [101]	4.714	0.0969
CC (Walters et al. 2004 [29])	4.899	0.0872

TABLE IX: ^1D resonance parameters for Ps-H scattering

Method	^1E_R (eV)	$^1\Gamma$ (eV)
Current work: Average ± standard deviation	5.1867 ± 0.0021	0.0125 ± 0.0003
Current work: S-matrix complex Kohn	5.1863	0.0125
Complex rotation (Ho and Yan 2000) [33]	5.1661 ± 0.0014	0.0174 ± 0.0027
CC (Walters et al. 2004 [29])	5.200	0.0095

TABLE X: ^1F resonance parameters for Ps-H scattering

D. Effective Range Theories

Prior work in the literature for ^1S Ps-H scattering [21, 42, 47] uses the ERT expansion for short-range interactions as given in Eq. (26) as well as the approximation to the scattering length given in Eq. (25). Table XI shows the $^{1,3}S$-wave scattering lengths and effective ranges given by Refs. [21, 29, 42, 47]. Some other calculations of the $^{1,3}S$ scattering lengths and effective ranges can be found in Refs. [40–42, 46]. These all agree reasonably well with each other. Additional calculations of $^{1,3}S$-wave scattering lengths and effective ranges can also be found in Refs. [37–39, 44, 45, 49, 102].

We also use Eq. (25) to determine the $^{1,3}S$ scattering lengths from the phase shifts of very small κ, given in Table XI. Van Reeth and Humberston [21] fitted their phase shifts to the ERT for short-range interactions, Eq. (26), for a range in κ up to 0.5. They gave in their paper a plot of $\kappa \cot \delta_0^{\pm}$ versus κ^2. We perform a similar plot, which is given in Fig. 12, but use the complex Kohn phase shifts that we compute. As obtained in Ref. [21], the singlet result $\kappa \cot \delta_0^{+}$ lies on a relatively straight line, but the triplet result $\kappa \cot \delta_0^{-}$ curves down at low values of κ^2.

We investigate the low-energy region in more detail. We fit the complex Kohn phase shifts to the ERT for short-range interactions, Eq. (26), for the range $\kappa = 0.1 - 0.5$, but in

addition, we fit the phase shifts to this ERT for a range of $\kappa = 0.001 - 0.009$. We compare the results of the scattering lengths and effective ranges for the two fits in Table XI. We find that there is little difference in the ^1S results and the ^3S scattering length, but there is significant difference in the ^3S effective range.

For the Eq. (30) result of r_0^+ in Table XI, we use our result of E_b that we give in Table II and and our result of a^+ that we obtain using Eq. (26) for the range $\kappa = 0.001 - 0.009$. This value of r_0^+ is smaller than the other values of r_0^+ that we give in Table XI.

Van Reeth and Humberston [21] added a κ^3 term to the ERT for short-range interactions because of the van der Waals interaction. They found that for the ^1S, adding this term made no significant change in the quality of the fit. However, for the ^3S, they found that the addition of the κ^3 term improved the fit but that the effective range was very sensitive to the energy range over which the fit was made.

In addition to the fits we perform using the ERT for short-range interactions, Eq. (26), we use the ERT of Eq. (27) that includes terms due to the van der Waals interaction. We find that for the range $\kappa = 0.001 - 0.009$, the inclusion of these extra terms makes no difference to the $^{1,3}S$ scattering lengths and only a small difference to the effective ranges.

We also apply the QDT for the van der Waals interaction of Gao [77], Eq. (28), using the equations given by Gao [78] of the expansion of K_ℓ^0, Eq. (29), and the expressions for the scattering lengths and effective range. We use $\kappa = 0.002$ and 0.003 for the fit of Eq. (29) and give the results in Table XI. The $^{1,3}S$ scattering lengths we obtain using this QDT are identical to the results we obtain from the approximation to the definition and of that we obtain using the ERT for short-range interactions and the ERT for the van der Waals interaction, both for the range $\kappa = 0.001 - 0.009$. The $^{1,3}S$ effective ranges we obtain using the QDT agrees well with the results of the two ERT fits, Eq. (26) and Eq. (27), for this smaller range in κ.

Model	κ	a^+	r_0^+	a^-	r_0^-
Approx. to def. - Eq. (25)	0.001	4.331 ± 0.012	—	2.137 ± 0.008	—
ERT Short - Eq. (26)	$0.1 - 0.5$	4.308 ± 0.003	2.275	2.162 ± 0.003	1.343
ERT Short - Eq. (26)	$0.001 - 0.009$	4.331 ± 0.012	2.197	2.137 ± 0.008	2.035
ERT vdW - Eq. (27)	$0.001 - 0.009$	4.331 ± 0.012	2.221	2.137 ± 0.008	2.139
QDT - Eqs. (28), (29)	$0.002, 0.003$	4.331 ± 0.012	2.210	2.136 ± 0.008	2.151
Eq. (30)	—	—	2.106	—	—
Kohn (721 terms) Eq. (25) [21]	—	4.334	—	2.143	—
Kohn extrapolated [21]	—	4.311	2.27	2.126	1.39
Kohn Eq. (26) [21]	up to 0.5	4.30	2.27	2.147	—
CC 14Ps14H [47]	—	4.41	2.19	2.06	1.47
CC 14Ps14H+H^- [29]	—	4.327	—	—	—
SVM [42]	—	4.34	2.39	2.22	1.29

TABLE XI: $^{1,3}S$ scattering lengths and effective ranges

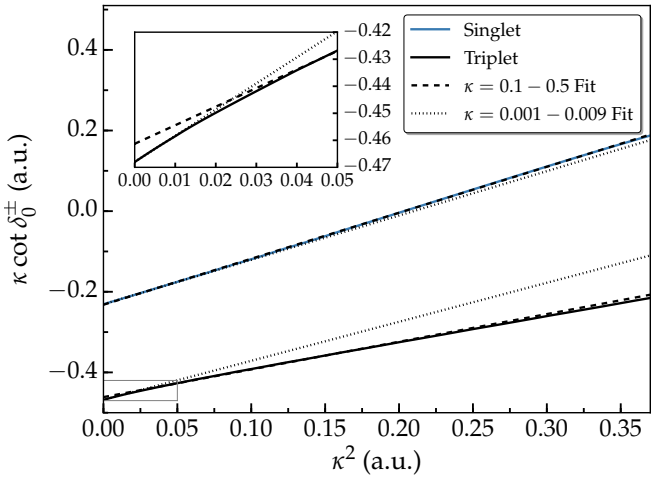

FIG. 12: (Color online) ^1S (upper lines) and ^3S (lower lines) phase shifts, plotted as $\kappa \cot \delta_0^{\pm}$ versus κ^2. The inset shows a magnified portion of the same data for low κ^2 as denoted by the gray box in the lower left.

Due to the van der Waals interaction, the ^1P- and ^3P-waves do not have effective ranges but do have scattering lengths [74]. Table XII gives the scattering lengths using the approximation to the definition of Eq. (25) and the QDT expressions we evaluate using the complex Kohn phase shifts at $\kappa = 0.01$. The scattering lengths obtained in these two different ways agree well for both the ^1P- and ^3P-waves. The $^{1,3}P$ scattering lengths have previously been computed by Ivanov et al. using their SVM phase shifts [42]. The results we obtain for the ^1P scattering length using the S-matrix complex Kohn phase shifts are comparable to the

^1P scattering length obtained with the SVM phase shifts. In contrast, the ^3P scattering lengths we determine differ significantly from the prior SVM results [42]. It seems that this difference can partly be attributed to the S-matrix complex Kohn phase shifts being larger than the SVM phase shifts.

Model	κ	a_1^+	a_1^-
Approx. to def. - Eq. (25)	0.01	-22.130 ± 0.173	1.4530 ± 0.1104
QDT - Eq. (28), (29)	0.01, 0.02	-22.200 ± 0.173	1.4158 ± 0.1107
SVM [42]	—	-20.7	6.80

TABLE XII: $^{1,3}P$ scattering lengths

V. CONCLUSION

We have extended the earlier Kohn and inverse Kohn variational calculations [21, 22] and have presented S-matrix complex Kohn variational results for Ps(1s) scattering from H(1s) below the Ps(n=2) threshold. We have determined highly accurate $^{1,3}S$ and $^{1,3}P$ phase shifts. The discrepancy in the D-wave phase shifts, especially the ^3D, between the complex Kohn variational and CC methods needs further investigation, such as explicitly including mixed symmetry terms into the trial wavefunction. Fortunately, the ^3D contribution to the elastic integrated cross section is small, and the ^1D resonance we compute with the complex Kohn phase shifts is reasonably good, providing some confidence in the reliability of the short-range part of the trial wavefunction describing the ^1D Ps-H scattering system at short distances. The $^{1,3}F$, $^{1,3}G$, and $^{1,3}H$ partial waves have very small phase shifts and do not contribute greatly to the elastic integrated or momentum transfer cross sections.

We have presented the elastic differential, elastic integrated, and momentum transfer cross sections using the S-matrix complex Kohn variational phase shifts for the first six partial waves. The elastic differential cross section is slightly backward peaked at low energy but quickly becomes strongly forward peaked as $E_{\boldsymbol{\kappa}}$ increases.

We have calculated resonance positions and widths for the ^1S, ^1P, ^1D, and ^1F partial waves using the Kohn variational method and its variants, which compare favorably with the complex rotation results of Refs. [30–33]. We have also provided a detailed investigation of the effective ranges and scattering lengths for $^{1,3}S$, along with the $^{1,3}P$ scattering lengths.

We have presented results using multiple effective range theories. The $^{1,3}S$ scattering lengths agree well with previous work [21, 29, 42, 47]. When we use a κ range of 0.1 to 0.5, we obtain a ^3S effective range close to those previously reported [21, 42, 47], but when we use smaller κ values, we obtain a noticeably larger result. While the complex Kohn ^1P scattering length agrees with the SVM [42], the complex Kohn ^3P scattering length is much smaller.

ACKNOWLEDGMENTS

We wish to thank Drs. Y. K. Ho, J. W. Humberston, K. Pachucki, Z.-C. Yan, and G. Peach for discussions. We appreciate files from Dr. Allan Todd and communications with Drs. Edward Armour, James Cooper, and Martin Plummer. We appreciate the referee's careful reading of the manuscript and for the issues the referee raised. S. J. W. acknowledges support from NSF under grant no. PHYS-0968638 and from UNT through the UNT faculty research grant GA9150. Computational resources were provided by UNT's High Performance Computing Services, a project of Academic Computing and User Services division of the University Information Technology with additional support from UNT Office of Research and Economic Development.

[1] B. L. Brown, "Creation of Monoenergetic Positronium (Ps) in a Gas," Bull. Am. Phys. Soc. **30**, 614 (1985).

[2] G. Laricchia, M. Charlton, S. A. Davies, C. D. Beling and T. C. Griffith, "The production of collimated beams of o-Ps atoms using charge exchange in positron-gas collisions," J. Phys. B **20**, L99 (1987).

[3] N. Zafar, G. Laricchia, M. Charlton, and A. Garner, "Positronium-Argon Scattering," Phys. Rev. Lett. **76**, 1595 (1996).

[4] A. J. Garner, G. Laricchia, and A. Özen, "Ps beam production and scattering from gaseous targets," J. Phys. B **29**, 5961 (1996).

[5] G. Laricchia, S. Armitage, Á. Kövér, and D.J. Murtagh, "Ionizing collisions by positrons and positronium impact on the inert atoms," in *Advances In Atomic, Molecular, and Optical Physics* (Elsevier BV, 2008) p. 1.

[6] A. J. Garner, A. Özen, and G. Laricchia, "The effect of forward-angle scattering on positronium-gas total cross sections," J. Phys. B **33**, 1149 (2000).

[7] S. Armitage, D. E. Leslie, A. J. Garner, and G. Laricchia, "Fragmentation of Positronium in Collision with He Atoms," Phys. Rev. Lett. **89**, 173402 (2002).

[8] G. Laricchia, S. Armitage, and D.E. Leslie, "Positronium induced collisions," Nucl. Instrum. Methods B **221**, 60 (2004).

[9] S. Armitage, D.E. Leslie, J. Beale, and G. Laricchia, "Collisions involving positronium," Nucl. Instrum. Methods B **247**, 98 (2006).

[10] J. J. Engbrecht, M. J. Erickson, C. P. Johnson, A. J. Kolan, A. E. Legard, S. P. Lund, M. J. Nyflot, and J. D. Paulsen, "Energy-dependent Ps-He momentum-transfer cross section at low energies," Phys. Rev. A **77**, 012711 (2008).

[11] S. J. Brawley, S. Armitage, J. Beale, D. E. Leslie, A. I. Williams, and G. Laricchia, "Electron-Like Scattering of Positronium," Science **330**, 789 (2010).

[12] A. J. Garner, A. Özen, and G. Laricchia, "Positronium beam scattering from atoms and molecules," Nucl. Instrum. Methods B **143**, 155 (1998).

[13] J. Beale, S. Armitage, and G. Laricchia, "Positronium- and positron-H_2O total cross sections," J. Phys. B **39**, 1337 (2006).

[14] D. M. Schrader, F. M. Jacobsen, N.-P. Frandsen, and U. Mikkelsen, "Formation of Positronium Hydride," Phys. Rev. Lett. **69**, 57 (1992).

[15] D. Woods, P. Van Reeth, and S. J. Ward, `http://meetings.aps.org/link/BAPS.2014.DAMOP.Q1.55`, `http://meetings.aps.org/link/BAPS.2014.MAR.W26.3` ().

[16] D. Woods, S. J. Ward, and P. Van Reeth, `http://meetings.aps.org/link/BAPS.2013.DAMOP.Q1.122`, `http://meetings.aps.org/link/BAPS.2013.MAR.J25.8`, `http://meetings.aps.org/link/BAPS.2012.DAMOP.U3.4`, `http://meetings.aps.org/link/BAPS.2011.DAMOP.Q1.88`, `http://meetings.aps.org/link/BAPS.2010.DAMOP.T1.165` ().

[17] S. J. Ward, D. Woods, and P. Van Reeth, `http://meetings.aps.org/Meeting/DAMOP15/Session/Q1.113`.

[18] D. Woods, P. Van Reeth, and S. J. Ward, "Elaborate Calculations of low-energy Ps-H collisions," in *Book of Abstracts, XVIII International Workshop on Low-Energy Positron and Postronium Physics & XIX International Symposium Electron-Molecule Collisions and Swarms, 17-20 July 2015, Lisbon, Portugal, POSMOL 2015; ISBN 978-989-20-5845-0*, edited

by Paulo Limão-Vieira, Filipino Ferrero da Silva, Guilherme Mendes, and Emanuele Langworthy, and Tiago Cunha; P. 44, p. 67.

[19] P. Van Reeth, J. W. Humberston, D. Woods, and S. J. Ward, "A comparison of positron, electron and positronium low-energy scattering from hydrogen," in *Book of Abstracts, XVIII International Workshop on Low-Energy Positron and Postronium Physics & XIX International Symposium Electron-Molecule Collisions and Swarms, 17-20 July 2015, Lisbon, Portugal, POSMOL 2015; ISBN 978-989-20-5845-0*, edited by Paulo Limão-Vieira, Filipino Ferrero da Silva, Guilherme Mendes, and Emanuele Langworthy, and Tiago Cunha; P. 41, p. 64.

[20] D. Woods, *Variational Calculations of Positronium Scattering with Hydrogen*, Ph.D. thesis, University of North Texas (in preparation).

[21] P. Van Reeth and J. W. Humberston, "Variational calculations of s-wave positronium-hydrogen scattering," J. Phys. B **36**, 1923 (2003).

[22] P. Van Reeth and J. W. Humberston, "Low energy positronium-hydrogen scattering," Nucl. Instrum. Methods B **221**, 140 (2004).

[23] R. R. Lucchese, "Anomalous singularities in the complex Kohn variational principle of quantum scattering theory," Phys. Rev. A **40**, 6879 (1989).

[24] J. N. Cooper, E. A. G. Armour, and M. Plummer, "Anomaly-free singularities in the generalized Kohn variational method," J. Phys. A **42**, 095207 (2009).

[25] J. N. Cooper, M. Plummer, and E. A. G. Armour, "Equivalence of the generalized and complex Kohn variational methods," J. Phys. A **43**, 175302 (2010).

[26] A. C. Todd, *Helium-Antihydrogen Interactions*, Ph.D. thesis, The University of Nottingham (2007).

[27] G. W. F. Drake and Z.-C. Yan, "Asymptotic-expansion method for the evaluation of correlated three-electron integrals," Phys. Rev. A **52**, 3681 (1995).

[28] Z.-C. Yan and G. W. F. Drake, "Computational methods for three-electron atomic systems in Hylleraas coordinates," J. Phys. B **30**, 4723 (1997).

[29] H. R. J. Walters, A. C. H. Yu, S. Sahoo, and S. Gilmore, "Positronium-atom collisions," Nucl. Instrum. Methods B **221**, 149 (2004).

[30] Z.-C. Yan and Y. K. Ho, "Ground state and S-wave autodissociating resonant states of positronium hydride," Phys. Rev. A **59**, 2697 (1999).

[31] Z.-C. Yan and Y. K. Ho, "P-wave autodissociating resonant states of positronium hydride,"

Phys. Rev. A **57**, R2270 (1998).

[32] Y. K. Ho and Z.-C. Yan, "A D-wave resonance in positronium-hydrogen scattering," J. Phys. B **31**, L877 (1998).

[33] Y. K. Ho and Z.-C. Yan, "F- and G-wave resonances in positronium-hydrogen scattering," Phys. Rev. A **62**, 052503 (2000).

[34] Y. K. Ho, "Positron annihilation in positronium hydrides," Phys. Rev. A **34**, 609 (1986).

[35] J. Mitroy, "Energy and expectation values of the PsH system," Phys. Rev. A **73**, 054502 (2006).

[36] S. Bubin and L. Adamowicz, "Nonrelativistic variational calculations of the positronium molecule and the positronium hydride," Phys. Rev. A **74**, 052502 (2006).

[37] B. A. P. Page, "Positronium-hydrogen scattering lengths," J. Phys. B **9**, 1111 (1976).

[38] R. J. Drachman and S. K. Houston, "Positronium-hydrogen elastic scattering," Phys. Rev. A **12**, 885 (1975).

[39] R. J. Drachman and S. K. Houston, "Positronium-hydrogen elastic scattering: The electronic S=1 state," Phys. Rev. A **14**, 894 (1976).

[40] S. Chiesa, M. Mella, and G. Morosi, "Orthopositronium scattering off H and He," Phys. Rev. A **66**, 042502 (2002).

[41] I. A. Ivanov, J. Mitroy, and K. Varga, "Elastic Positronium-Atom Scattering Using the Stochastic Variational Method," Phys. Rev. Lett. **87**, 063201 (2001).

[42] I. A. Ivanov, J. Mitroy, and K. Varga, "Positronium-hydrogen scattering using the stochastic variational method," Phys. Rev. A **65**, 032703 (2002).

[43] P. K. Sinha, P. Chaudhury and A. S. Ghosh, "Ps-H scattering using the three-state positronium close-coupling approximation," J. Phys. B **30**, 4643 (1997).

[44] C. P. Campbell, M. T. McAlinden, F. G. R. S. MacDonald, and H. R. J. Walters, "Scattering of Positronium by Atomic Hydrogen," Phys. Rev. Lett. **80**, 5097 (1998).

[45] S. K. Adhikari and P. K. Biswas, "Positronium–hydrogen-atom scattering in a five-state model," Phys. Rev. A **59**, 2058 (1999).

[46] P. K. Sinha, A. Basu, and A. S. Ghosh, "Low-energy positronium-hydrogen elastic scattering using the six-state close coupling approximation," J. Phys. B **33**, 2579 (2000).

[47] J. E. Blackwood, M. T. McAlinden, and H. R. J. Walters, "Positronium scattering by atomic hydrogen with inclusion of target excitation channels," Phys. Rev. A **65**, 032517 (2002).

[48] J. E. Blackwood, M. T. McAlinden, and H. R. J. Walters, "Importance of the H^- channel in Ps-H scattering," Phys. Rev. A **65**, 030502(R) (2002).

[49] S. Hara and P. A. Fraser, "Low-energy ortho-positronium scattering by hydrogen atoms," J. Phys. B **8**, L472 (1975).

[50] H. Ray and A. S. Ghosh, "Positronium-hydrogen-atom scattering using the static exchange model," J. Phys. B **30**, 3745 (1997); "Positronium-hydrogen atom scattering using the static exchange model," J. Phys. B **29**, 5505 (1996).

[51] H. S. W. Massey and C. B. O. Mohr, "Gaseous Reactions involving Positronium," Proc. Phys. Soc. A **67**, 695 (1954).

[52] J. R. Oppenheimer, "On the Quantum Theory of Electronic Impacts," Phys. Rev. **32**, 361 (1928).

[53] S. Geltman, *Topics in Atomic Collision Theory* (Academic Press, New York and London, 1969).

[54] N. F. Mott and H. S. W. Massey, *The Theory of Atomic Collisions*, 3rd ed. (Clarendon Press, Oxford, 1965).

[55] B. H. Bransden and C. J. Joachain, *Physics of Atoms and Molecules* (Pearson Education Limited, Harlow, England, 2003).

[56] B. H. Bransden, *Atomic Collision Theory* (W. A. Benjamin, Inc., New York, 1970).

[57] Mary T. McAlinden, F. G. R. S. MacDonald, and H.R.J. Walters, "Positronium-atom scattering," Can. J. Phys. **74**, 434 (1996).

[58] J.-Y. Zhang, Z.-C. Yan, and U. Schwingenschlögl, "Elastic scattering of positronium: Application of the confined variational method," EPL **99**, 43001 (2012).

[59] P. J. Mohr, B. N. Taylor, and D. B. Newell, "CODATA recommended values of the fundamental physical constants: 2010," Rev. Mod. Phys. **84**, 1527 (2012); "NIST Conversions," `http://physics.nist.gov/cuu/Constants/energy.html` (2014), accessed: 2014-08-27.

[60] P. Van Reeth and J. W. Humberston, "Elastic scattering and positronium formation in low-energy positron-helium collisions," J. Phys. B **32**, 3651 (1999).

[61] P. Van Reeth, *Theoretical Studies of Positronium Formation in Low Energy Positron-Helium Collisions*, Ph.D. thesis, University College London (1996).

[62] C. Schwartz, "Lamb Shift in the Helium Atom," Phys. Rev. **123**, 1700 (1961).

[63] C. J. Brown and J. W. Humberston, "Positronium formation in positron-hydrogen scatter-

ing," J. Phys. B **18**, L401–L406 (1985).

[64] C. J. Brown, *The Interactions of Low Energy Positrons with Atomic Hydrogen*, Ph.D. thesis, University College London (1986).

[65] M. S. T. Watts, *Theoretical Studies of Positronium Formation in Positron Collisions with Lithium and Hydrogen Atoms*, Ph.D. thesis, University College London (1994).

[66] J. W. Humberston, P. Van Reeth, M. S. T. Watts, and W. E. Meyerhof, "Positron-hydrogen scattering in the vicinity of the positronium formation threshold," J. Phys. B **30**, 2477 (1997).

[67] P. Van Reeth and J. W. Humberston, "A partial-wave analysis of positronium formation in positron-helium scattering," J. Phys. B **30**, L95 (1997).

[68] E. A. G. Armour and J. W. Humberston, "Methods and programs in collisions of positrons with atoms and molecules," Phys. Rep. **204**, 165 (1991).

[69] P. Van Reeth and J. W. Humberston, unpublished (2015).

[70] H. A. Bethe, "Theory of the Effective Range in Nuclear Scattering," Phys. Rev. **76**, 38 (1949).

[71] J. M. Blatt and J. D. Jackson, "On the Interpretation of Neutron-Proton Scattering Data by the Schwinger Variational Method," Phys. Rev. **76**, 18 (1949).

[72] I. I. Fabrikant and G. F. Gribakin, "Similarity between Positronium-Atom and Electron-Atom Scattering," Phys. Rev. Lett. **112**, 243201 (2014).

[73] C. K. Au and R. J. Drachman, "van der Waals Force Between Positronium and Hydrogenic Atoms: Finite-Mass Corrections," Phys. Rev. Lett. **56**, 324 (1986).

[74] B. R. Levy and J. B. Keller, "Low-Energy Expansion of Scattering Phase Shifts for Long-Range Potentials," J. Math. Phys. **4**, 54 (1963).

[75] M. R. Flannery, *Springer Handbook of Atomic, Molecular, and Optical Physics*, 2nd ed., edited by G. W. F. Drake (Springer, New York, NY, 2006) p. 668.

[76] D. W. Martin and P. A. Fraser, "The van der Waals force between positronium and light atoms," J. Phys. B **13**, 3383 (1980).

[77] B. Gao, "Solutions of the Schrödinger equation for an attractive $1/r^6$ potential," Phys. Rev. A **58**, 1728 (1998).

[78] B. Gao, "Quantum-defect theory of atomic collisions and molecular vibration spectra," Phys. Rev. A **58**, 4222 (1998).

[79] K. Pachucki, M. Puchalski, and E. Remiddi, "Recursion relations for the generic Hylleraas three-electron integral," Phys. Rev. A **70**, 032502 (2004).

[80] D. Woods, N. Weber, M. Dario, and M. Týč, "Developer's Image Library," `http://openil.sourceforge.net` (2009).

[81] A. Lüchow and H. Kleindienst, "An efficient basis selection procedure for the reduction of the dimension in large Hylleraas-CI calculations," Chem. Phys. Lett. **197**, 105 (1992).

[82] E. Anderson, Z. Bai, C. Bischof, S. Blackford, J. Demmel, J. Dongarra, J. Du Croz, A. Greenbaum, S. Hammarling, A. McKenney, and D. Sorensen, *LAPACK Users' Guide*, 3rd ed. (Society for Industrial and Applied Mathematics, Philadelphia, PA, 1999).

[83] G. Breit and E. Wigner, "Capture of slow neutrons," Phys. Rev. **49**, 519 (1936).

[84] J. Macek, "Behavior of Eigenphases near a Resonance," Phys. Rev. A **2**, 1101 (1970).

[85] A. U. Hazi, "Behavior of the eigenphase sum near a resonance," Phys. Rev. A **19**, 920 (1979).

[86] MATLAB, *version 8.3.0 (R2014a)* (The MathWorks Inc., Natick, Massachusetts, 2014).

[87] P.K. Biswas, "Effect of H^- ion formation on positronium-hydrogen elastic scattering," J. Phys. B **34**, 4831 (2001).

[88] P. A. Fraser, "The Scattering of Low-energy Ortho-positronium by Hydrogen Atoms," Proc. Phys. Soc. **78**, 329 (1961).

[89] "CurveSnap," `https://github.com/xoofee/CurveSnap` (2014), accessed: 2014-08-27.

[90] C. J. Joachain, *Quantum collision theory* (North-Holland, Amsterdam Oxford, 1979) p. 291.

[91] Y. Wang, O. Zatsarinny, and K. Bartschat, "B-spline R-matrix-with-pseudostates calculations for electron-impact excitation and ionization of nitrogen," Phys. Rev. A **89**, 062714 (2014).

[92] R.P. McEachran and A. D. Stauffer, "Momentum transfer cross sections for the heavy noble gases," Eur. Phys. J. D **68**, 153 (2014).

[93] Y. Nagashima, T. Hyodo, K. Fujiwara, and A. Ichimura, "Momentum-transfer cross section for slow positronium-He scattering," J. Phys. B **31**, 329 (1998).

[94] F. Saito, Y. Nagashima, and T. Hyodo, "Momentum-transfer cross sections for slow positroniumgas collisions," J. Phys. B **36**, 4191 (2003).

[95] M. Skalsey, J. J. Engbrecht, R. K. Bithell, R. S. Vallery, and D. W. Gidley, "Thermalization of positronium in gases," Phys. Rev. Lett. **80**, 3727 (1998).

[96] J. E. Blackwood, M. T. McAlinden, and H. R. J. Walters, "Positronium scattering by Ne, Ar, Kr and Xe in the frozen target approximation," J. Phys. B **35**, 2661 (2002).

[97] H. S. W. Massey, E. H. S. Burhop, and H. B. Gilbody, *Electronic and Ionic Impact Phe-*

nomena, Volume I, 2nd ed., edited by H. S. W. Massey and E. H. S. Burhop (Oxford at the Clarendon Press, Oxford, 1969) p. 47.

[98] R. J. Drachman, "Autodissociating Rydberg states of positronium hydride," Phys. Rev. A **19**, 1900 (1979).

[99] A. U. Hazi and H. S. Taylor, "Stabilization Method of Calculating Resonance Energies: Model Problem," Phys. Rev. A **1**, 1109 (1970).

[100] H. Ray, "Findings in Ps-H scattering," Phys. Rev. A **73**, 064501 (2006).

[101] Z.-C. Yan and Y. K. Ho, "Determination of resonance energies and widths in Ps-H scattering using the stabilization method," J. Phys. B **36**, 4417 (2003).

[102] S. K. Adhikari and P. Mandal, "Convergent variational calculation of positronium-hydrogen-atom scattering lengths," J. Phys. B **34**, L187 (2001).